The Mechanochemistry of V-ATPase Proton Pumps

Michael Grabe,* Hongyun Wang,† and George Oster†
*Departments of Physics and †Molecular and Cellular Biology and College of Natural Resources, University of California, Berkeley, California 94720-3112 USA

ABSTRACT The vacuolar H^+-ATPases (V-ATPases) are a universal class of proton pumps that are structurally similar to the F-ATPases. Both protein families are characterized by a membrane-bound segment (V_o, F_o) responsible for the translocation of protons, and a soluble portion, (V_1, F_1), which supplies the energy for translocation by hydrolyzing ATP. Here we present a mechanochemical model for the functioning of the V_o ion pump that is consistent with the known structural features and biochemistry. The model reproduces a variety of experimental measurements of performance and provides a unified view of the many mechanisms of intracellular pH regulation.

INTRODUCTION

One of the defining characteristics of intracellular membrane compartments is the difference between their lumenal pH and that of the bulk cytoplasm. This pH differential is maintained principally by the vacuolar ATPases. These proteins comprise a class of proton pumps that bear a high degree of structural homology to the F-ATPases that manufacture ATP using the proton-motive force across the mitochondrial inner membrane (Engelbrecht and Junge, 1997; Finbow and Harrison, 1997; Kibak et al., 1992; Nelson, 1992; Taiz and Nelson, 1996). Indeed, bacterial F-ATPases can, under anaerobic conditions, reverse themselves to function as proton pumps. Building on this structural similarity, we present here a quantitative model for the V-ATPase proton pump, and demonstrate that it can reproduce many of the experimentally measured properties.

Recently there has been a flood of new information on the structure, mechanics, and biochemistry of the F-ATPases. The crystal structure of F_1 determined by John Walker's laboratory lent strong support to Boyer's "binding change" model that posited that the three catalytic sites alternated their activity in a rotational sequence (Abrahams et al., 1994; Boyer, 1997). This was dramatically confirmed by the startling visual demonstration that F_1 was indeed a rotary motor (Kinosita et al., 1999; Noji et al., 1997). The Japanese group also determined that the rotation of the F_1 motor advanced in three steps per revolution, with each step requiring the hydrolysis of one ATP, and that the motor developed an average torque of over 40 pN · nm. Amazingly, the work done against the average drag torque in a single rotation was nearly equal to the free energy drop accompanying the hydrolysis of three ATPs, indicating that the F_1 motor operates at nearly 100% efficiency. Wang and Oster combined the structural, biochemical, and mechanical data into a unified mechanochemical model for the F_1 motor (Wang and Oster, 1998).

Because it is largely a transmembrane structure, information on the F_o portion of ATP synthase has been more difficult to obtain. Recently, Sambongi et al. (1999) provided visual proof that the c-subunit oligomer rotated along with the γ-subunit shaft that connects it to the F_1 hexamer. Structures for the c-subunit oligomer have been deduced from NMR (Rastogi and Girvin, 1999) and x-ray crystallography studies (Stock et al., 1999). While they do not agree in all details, it is clear that the F_o motor consists of 10 or 12 subunits with rotational symmetry, as deduced from a variety of studies from several laboratories (Fillingame et al., 1999; Long et al., 1998; Nakamoto et al., 1999). To counter the large torque developed by the F_1 motor in hydrolysis mode, the F_o motor must generate an even larger torque in the opposite direction to synthesize ATP. It does this by converting the transmembrane proton-motive force into rotary motion. Various qualitative models for this energy transduction have been proposed (Junge et al., 1997; Vik and Antonio, 1994), and Elston et al. (1998) formulated a quantitative model that explained the torque generation mechanism as an "electrostatic Brownian ratchet."

The model for the V-ATPase we propose herein is built on the assumption that the structural similarities between the F- and V-ATPases reflect a mechanistic similarity in their operation. Indeed, in their model for the F_o motor, Elston et al. (1998) showed that, when driven in reverse, the F_o motor could indeed function as a proton pump, albeit not a very effective one. Here we shall show that by modifying that model in accordance with the known structural properties of the V-ATPases, we can construct a mechanochemical model for the vacuolar proton pumps that is in quantitative agreement with a variety of experimental observations. First, however, we briefly review the similarities between the two protein classes to buttress this fundamental assumption.

Both the V- and F-ATPase protein families consist of two major portions: a membrane-spanning portion (V_o, F_o) containing the proton channel, and a soluble portion (V_1, F_1) containing the nucleotide binding sites. Fig. 1 illustrates the

Received for publication 3 August 1999 and in final form 22 February 2000.

Address reprint requests to Dr. George Oster, 201 Wellman Hall, University of California, Berkeley, CA 94720-3112. Tel.: 510-642-5277; Fax: 510-642-7428; E-mail: goster@nature.berkeley.edu.

0006-3495/00/06/2798/16 $2.00

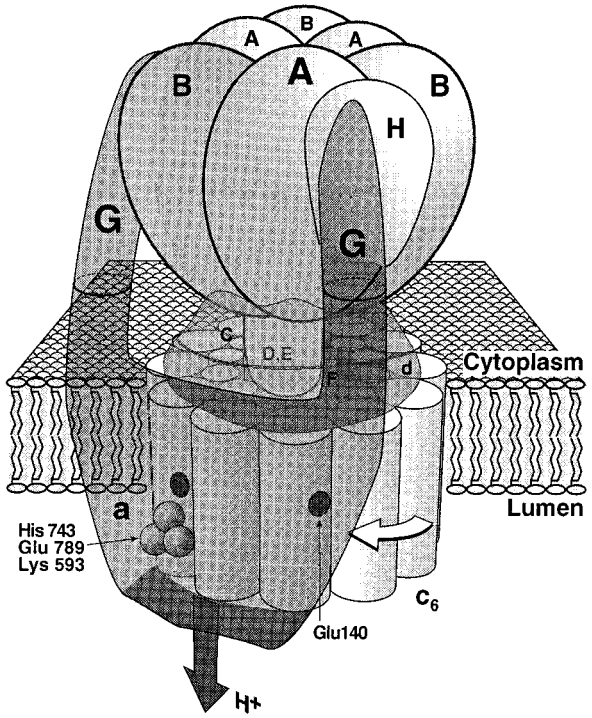

FIGURE 1 Schematic structure of the V-ATPase proton pump. The correspondence between the F and V-ATPase notation is summarized in the table below. Those connections that are more speculative are accompanied by a question mark. Molecular weights are given in parentheses for *Neurospora crassa* (Margolles-Clark et al., 1999). The V_1 portion consists of subunits (A_3, B_3, C, D, E, F, G_2, H). The $(AB)_3$ hexamer contains the ATP binding sites. The V_o portion consists of subunits (a, d, c_6, c′, c″). The subunits c′ and c″ are not represented in this picture since their role and stoichiometry are presently unclear (Margolles-Clark et al., 1999). The proton channel is formed in part by the a-subunit, which is composed of approximately nine transmembrane α-helices. The key charges that participate in proton transport are Lys-593, His-743, and Glu-789 on a-subunits and the six proton binding sites (Glu-140) on the c-subunits, each of which consists of four transmembrane α-helices. The counter-rotating subunits are denoted by convention as the rotor (c_6CDE) and stator ($A_3B_3aG_2$). Hydrolysis in V_1 drives the rotation of the c subunit with respect to the a-subunit (indicated by the *arrow*). This drives protons from the basic reservoir (cytoplasm) to the acidic reservoir (lumen).

V-ATPase	a (98)	A (67)	B (57)	F (13)	D (28), E (26)	c (16)	G (13)
F-ATPase *(E. coli)*	a?	β	α	ϵ?	γ?	c	b

overall geometry of the V-ATPase proton pumps and summarizes the subunit notation for both protein families (Stevens and Forgac, 1997). The soluble portions of both ATPases have a sixfold symmetry created by the alternation of A and B subunits in V_1 and the β and α subunits in F_1. A and B share 25% sequence identity with β and α, respectively (Bowman et al., 1988a, b; Zimniak et al., 1988). In addition, each hexamer contains three catalytic sites capable of ATP hydrolysis (Arai et al., 1988). An important difference between the F- and V-ATPases lies in the structure of the c-subunits of (V_o, F_o)). In the F-ATPases 10–12 c-subunits are arranged in a ring; each c-subunit consists of a double α-helix; α-helix 2 of each subunit contains an acidic proton binding site (Asp-61, *Escherichia coli numbering*). The corresponding structure in the V-ATPases comprises six c-subunits; each c-subunit consists of four transmembrane α-helices; helix 4 has an acidic proton binding site (Glu-140, *Saccharomyces cerevisiae numbering*). Each of the acidic sites on V_o binds a proton in an electrostatic well whose depth is related to its *in situ* pK_a values by $V/k_BT = -2.3$ pK_a (k_B is Boltzmann's constant and T the absolute temperature). Thus the F-ATPases have 12 proton carriers, while the V-ATPases have 6. This has important consequences for the pump's behavior, as we shall see (Arai et al., 1988; Dmitriev et al., 1995; Groth and Walker, 1997; Holzenburg et al., 1993). The strong resemblance of the two enzymes in all areas but the c-subunit stoichiometry has led to the hypothesis that V_o evolved by gene fusion and mutation in the c-subunits of F_o, resulting in the loss of one of the two initial carboxyl residues involved in transport (Cross and Taiz, 1990). This occurred without major change in the soluble ATP binding hexamer.

The a subunit in F_o is likely composed of five transmembrane α-helices, and contains a critical basic residue (Arg-210) on helix 4 (Valiyaveetil and Fillingame, 1997). In addition to forming a path for protons across the membrane, subunit a is thought to interact electrostatically with protons bound to subunit c (Fillingame, 1990). The VPH1 gene encodes the a subunit of V_o (called the Vph1p subunit in yeast). This polypeptide contains three amino acids, Lys-593, His-743, and Glu-789, in putative membrane-spanning domains that when mutated result in reduced proton transport and ATPase activity (Leng et al., 1996, 1999). This has prompted researchers to suggest that the charged residues play a fundamental role in the mechanism of ion translocation, and that the a-subunit forms part of the proton-conducting pathway through the membrane (Finbow and Harrison, 1997; Margolles-Clark et al., 1999). We adopt this structural interpretation and assume that the a-subunit serves the same function in both V- and F-ATPase.

A MECHANOCHEMICAL MODEL OF THE V-ATPase PROTON PUMP

In this section we present a quantitative model for the V-ATPase proton pump. We base our analysis on the close structural similarities between the F- and V-ATPases. The conventional paradigm for active transmembrane ion transport is the "alternating access" mechanism: ions are bound tightly on the low concentration side and a conformational change exposes them to the high concentration side, weakening their binding affinity so that they dissociate. The pump then resets its conformation to repeat the cycle (Alberts et al., 1994; Eisenberg and Hill, 1985). The energy to drive the cycle is supplied by nucleotide hydrolysis or a complementary ion gradient. The structural basis of the conformational change that implements the alternating access has not been worked out for any ion pump. Here we construct a model of the V-ATPase proton pumps assuming the conformational change is a simple rotation.

Model geometry

Like the F-ATPases, it is believed the V-ATPase structure can be subdivided into a counter-rotating "stator" and "rotor" (Boekema et al., 1997; Elston et al., 1998; Fillingame, 1996; Forgac, 2000; Harrison et al., 1997; Junge et al., 1997; Vik and Antonio, 1994). The rotor is likely to consist of the c-, D-, and E-subunits. The stator is thought to be composed of the a-subunit, the $(AB)_3$ hexamer, a connecting unit analogous to the $b_2\delta$ proteins in F-ATPase, and possibly H (Boekema et al., 1997; Graham and Stevens, 1999; Stevens and Forgac, 1997). Physically, a connecting unit, speculated to be subunit G, is essential to prevent the $(AB)_3$ hexamer from turning with the rotor. However, G lacks a membrane-spanning domain, which is present in subunit b, and it is likely present in two separate copies per enzyme (Boekema et al., 1999). It has been suggested that G binds tightly to a membrane-bound subunit, since it lacks this anchoring span (Margolles-Clark et al., 1999; Superkova et al., 1995).

Assuming that proton translocation involves a rotation of V_o in the membrane, there are several structural features that must be present for pumping to occur. Within the context of our model, we now discuss the biochemical and structural environment that the proton must experience for translocation. This discussion has little experimental support since it involves membrane proteins for which high-resolution structures are difficult to obtain. Notwithstanding, physical principles tell us that the true description must be similar to one of the two following scenarios.

Two models have been suggested for the rotor-stator assemblies, a two-channel model and a one-channel model (Dimroth et al., 1999; Elston et al., 1998; Junge et al., 1997; Vik and Antonio, 1994). Fig. 2 shows a face-on view of both models. In both, hydrolysis of ATP in V_1 by the $(AB)_3$ hexamer provides the torque that turns the rotor to the left (i.e., clockwise viewed from the cytoplasm). We shall not address the mechanism by which V_1 generates torque; for the purposes of this study we can represent V_1 by its load-velocity characteristic. To compute this we shall assume that the V_1 motor works the same way as the F_1-ATPase described in Oster and Wang (2000) and Wang and Oster (1998). As the rotor turns, protons are pumped from the basic reservoir (*top*) through the stator to the acid reservoir (*bottom*). Both of the configurations shown in Fig. 2 operate on the same "alternating access" principle discussed below (Alberts et al., 1994). The primary difference lies in the path the protons take in traversing the stator (shown by the *dashed lines* in Fig. 2). However, both pump models perform almost identically.

The interface between the rotor and stator must present a hydrophobic barrier to prevent proton leakage between the reservoirs; thus, there can be no direct proton path through the stator. The one- and two-channel models shown in Fig. 2 accomplish this somewhat differently. In the one-channel model, the six rotor acidic sites are located above the level of the membrane so that they are always in equilibrium with the basic reservoir outside of the stator. By contrast, the acidic sites in the two-channel model are located near the midplane of the membrane. In this position a rotor site can only be protonated from the basic reservoir when it enters the input channel within the rotor-stator interface; at all other positions rotor sites are buried in the lipid membrane and cannot communicate with either reservoir. In both models the output (acidic) channel extends into the stator to the level of the rotor proton binding sites. Thus the path of a proton in the one-channel model is short, while in the two-channel model a proton must board the rotor and make a complete circuit as the rotor turns before exiting the output channel.

The hydrophobic interface prevents unprotonated rotor sites from rotating to the left out of contact with the cytoplasm (see Eq. 21 in Appendix D) while a protonated rotor site can pass into the hydrophobic rotor-stator interface and enter the output channel. However, the rotor site will not release its proton unless its pK_a is reduced considerably. This is accomplished by the trio of stator charges (Lys-593, His-743, and Glu-789) since we assume that they lie near the path of the rotor sites. As a protonated site approaches the stator charges its pK_a is reduced, forcing it to relinquish its proton to the output channel. The trio of stator charges can be modeled by a single "equivalent" charge (see Eq. 20 in Appendix D). A polar hydrophilic strip connects the output channel to the basic reservoir, as shown in Fig. 2, to permit the passage of unprotonated rotor sites. The stator charge blocks proton leakage along this path.

Since the structure of the a-subunit is not well characterized, it is difficult to determine which stator assembly, if either, is correct. The one channel model describes experiments performed on the sodium F-ATPase; however, it requires exposing hydrophobic sections of the c-subunits to water (Dimroth et al., 1999). The more widely accepted two-channel model that places the rotor sites in the lipid bilayer cannot explain the sodium exchange experiments in the sodium F-ATPase (Kaim and Dimroth, 1999). In Dimroth *et al.* (1999) we have shown that the operating principle of the F_o motor is the same for both geometries. Similarly, the operating principle of the V_o pump is the same for both geometries, and so we have adopted the more widely accepted two-channel geometry shown in Fig. 2*b*.

The two-channel proton pump model works according to the following sequence of events shown in Fig. 3. The torque generated by V_1 moves a protonated rotor site out of the lipid bilayer and across the hydrophobic interface into the acidic channel. If the site enters the polar strip still protonated, the stator charge will reduce its pK_a, forcing it to relinquish its proton to the acidic reservoir. The site is then captured by the stator charge. The torque from V_1 is sufficient to surmount the electrostatic attraction between the rotor and stator charges and rotate the empty site into the basic reservoir. Until a rotor site is protonated, the torque generated by V_1 is insufficient to force it through the hydrophobic barrier at the channel stator interface. However, once neutralized by protonation, the site can be rotated across the barrier and into the bilayer (see Note 1 at end of text preceding appendices). While this scenario sounds reasonable, the only way to verify that the pump will operate as described is to construct a quantitative model, which we now proceed to do.

Mathematical formulation of the model

We describe the rotor position by its rotation angle, $\theta(t)$. A rotor site can be empty (charged) or occupied (nearly neutral). Thus the chemical state of a rotor site can be described by the binary variable $\mathbf{s}_i$ = (Empty, Full), $i = 1, \ldots, 6$. However, we need only keep track of those sites that interact with the stator. Since the rotor charges are spaced $\theta = 2\pi/6$ apart, the stator spans at most two sites; thus it is sufficient to follow the protonation status of four sites spanning the stator interface. Then the rotor state, denoted **s,** is determined by the states of these four sites, and can take on $2^4 = 16$ values. Since the association and dissociation of protons from rotor sites is much faster than the motion of the rotor, we can model the transitions between rotor ionization states as a Markov chain. As it passes through the stator, a rotor site encounters different physical environments: the polar strip, output channel, hydrophilic interface, and basic reservoir. Therefore, the binding and dissociation of protons from a rotor site depend on its angular position, θ; it can be described by the Markov equation

$$\frac{d\mathbf{s}}{dt} = \mathbf{K}(\theta)\mathbf{s} \tag{1}$$

Here $\mathbf{K}(\theta)$ is the transition matrix between chemical states, i.e., the proton association and dissociation rates from the rotor sites. A full description of $\mathbf{K}(\theta)$ and its elements is given in Appendix C.

The motion of the rotor can be computed from a force balance equating the viscous drag on the rotor to the torques that act on the rotor and the Brownian force modeling the rotor's thermal fluctuations, (i.e., Langevin's equation) (Risken, 1989):

$$\underbrace{\zeta \frac{d\theta}{dt}}_{\substack{\text{Frictional}\\ \text{drag}}} = \underbrace{\tau_Q(\theta, \mathbf{s})}_{\substack{\text{Rotor-stator}\\ \text{charge interaction}}} + \underbrace{\tau_{\Delta\Psi}(\theta, \mathbf{s})}_{\substack{\text{Membrane}\\ \text{potential}}} + \underbrace{\tau_{\Delta\epsilon}(\theta, \mathbf{s})}_{\substack{\text{Dielectric}\\ \text{barrier}}} + \underbrace{-\tau_D(\theta)}_{\substack{\text{Driving torque}\\ \text{from } V_1}} + \underbrace{\tau_B(t)}_{\substack{\text{Brownian}\\ \text{torque}}}, \quad \underbrace{\mathbf{s} = 1, \ldots, 16}_{\substack{\text{Chemical}\\ \text{states}}} \tag{2}$$

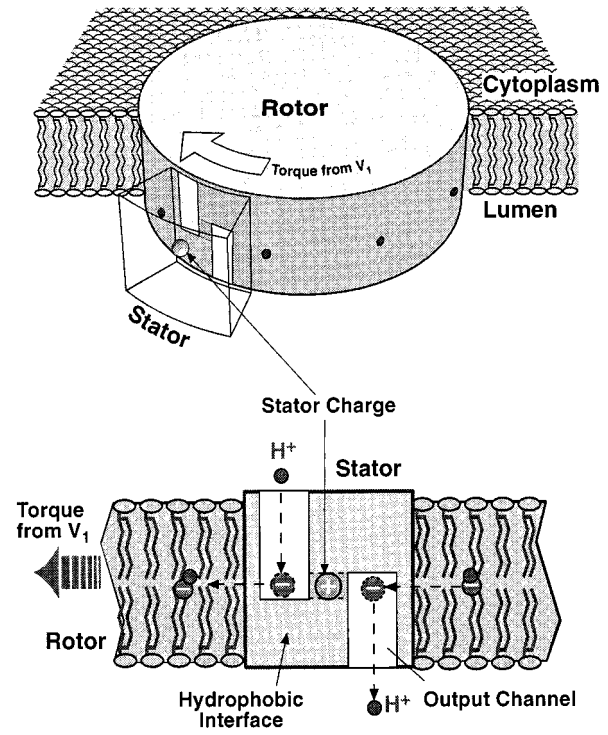

A

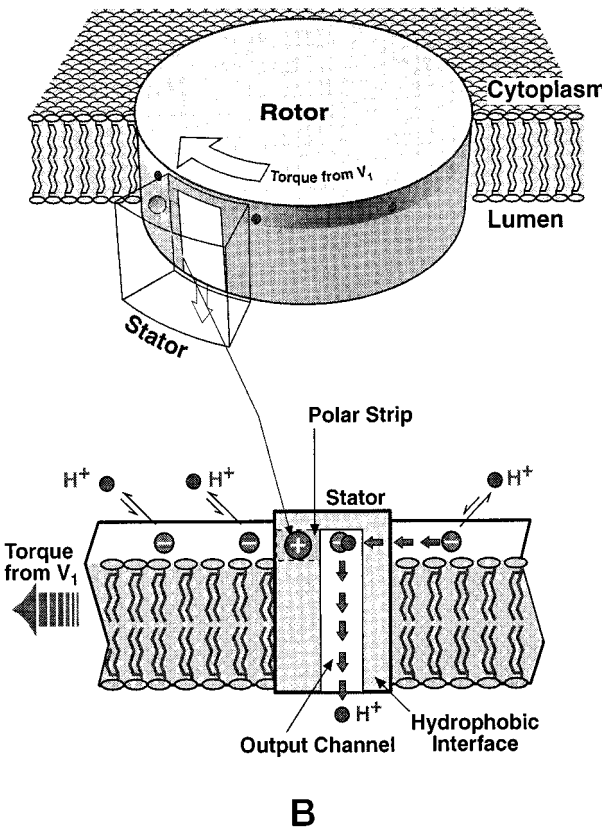

B

The terms in Eq. 2 are as follows; the explicit forms are given in Appendix D.

- The left-hand side is the viscous drag torque on the rotor. $d\theta/dt$ is the rotational velocity. ζ is the drag coefficient of the rotor treated as a cylinder rotating in the plane of the membrane;
- $\tau_Q(\theta, \mathbf{s})$ is the torque due to the electrostatic interaction between the stator charge and the rotor sites that are within the hydrophilic rotor-stator strip. Because of the high dielectric constant in the aqueous environment of the cytoplasm and the proton channels, this interaction is negligible except when the rotor site is within the polar strip. The charged (unoccupied) site will be attracted by the stator charge according to Coulomb's law corresponding to the dielectric and shielding environment of the stator;
- $\tau_{\Delta\Psi}(\theta, \mathbf{s})$ is the electrostatic torque on unoccupied rotor sites due to the membrane potential drop across the horizontal segment between the acidic channel and the basic reservoir;
- $\tau_{\Delta\epsilon}(\theta, \mathbf{s})$ is the electrostatic barrier that opposes the entry of a charged site into the hydrophobic rotor-stator interface. The height of this barrier is given approximately by $\sim 200\ (1/\epsilon_s - 1/\epsilon_c) \approx 45\ k_BT \approx 27$ kcal/mol (k_B is Boltzmann's constant, and T the absolute temperature), where $\epsilon_c \sim 80$ and $\epsilon_s \sim 4$ are the dielectric constants of the cytoplasm and the rotor-stator interface, respectively (Israelachvili, 1992);
- $\tau_D(\theta)$ is the torque exerted on the rotor from V_1 as it hydrolyzes ATP. This torque is transmitted via the rotating shaft (D, E) to the rotor while the stator is connected through the G subunit to the $(AB)_3$ hexamer;
- $\tau_B(t)$ is the random Brownian torque due to the thermal fluctuations of the rotor.

As indicated by their dependence on **s,** the electrostatic torques depend on the chemical state of the rotor site; that is, whether the site is charged (unoccupied) or uncharged (occupied). The model equations were solved numerically in the Fokker-Planck representation; the mathematical details are given in Appendix E. In the next section we present the results of these simulations.

Protons can "slip" past the stator

At modest transmembrane pH differences, each ATP hydrolyzed transports two protons across the membrane. That is, one revolution of the rotor

FIGURE 2 Perspective and face-on views of the rotor-stator assembly for the one- and two-channel models showing the paths protons follow in moving from the cytoplasm (*top*) into the lumen (*bottom*). Torque supplied by V_1 from ATP hydrolysis turns the rotor to the left (clockwise viewed from the cytoplasm in Fig. 1). (*a*) The two-channel model for the a-subunit. Two half-channels penetrate the stator to the level of the rotor sites; all other parts of the rotor-stator interface are hydrophobic. A horizontal polar strip connects the channels to allow the passage of an unprotonated site, but protons are blocked from leaking by the stator charge. Protons enter the input (basic) channel and bind to a rotor site, largely neutralizing it. Rotation carries the protonated site one complete revolution (to the left) where the site enters the output (acidic) channel (from the right). The stator charge forces the site to relinquish its proton into the lumen. Note that the sizes of the rotor and stator are such that two rotor sites cannot fit in the rotor-stator interface at once. (*b*) The one-channel model for the a-subunit. The rotor sites now lie above the level of the membrane and are in equilibrium with the cytoplasm when not in the stator. A single channel penetrates the stator to the level of the rotor sites; all other parts of the rotor-stator interface are hydrophobic. A horizontal polar strip connects the channel to the cytoplasm to allow passage of an unloaded site. The stator charge blocks passage of protons through the strip. Rotation brings a protonated site into the output channel where the stator charge forces it to release its proton to the lumen. The unloaded site then rotates through the polar strip, past the stator charge, exiting the rotor-stator interface to the left.

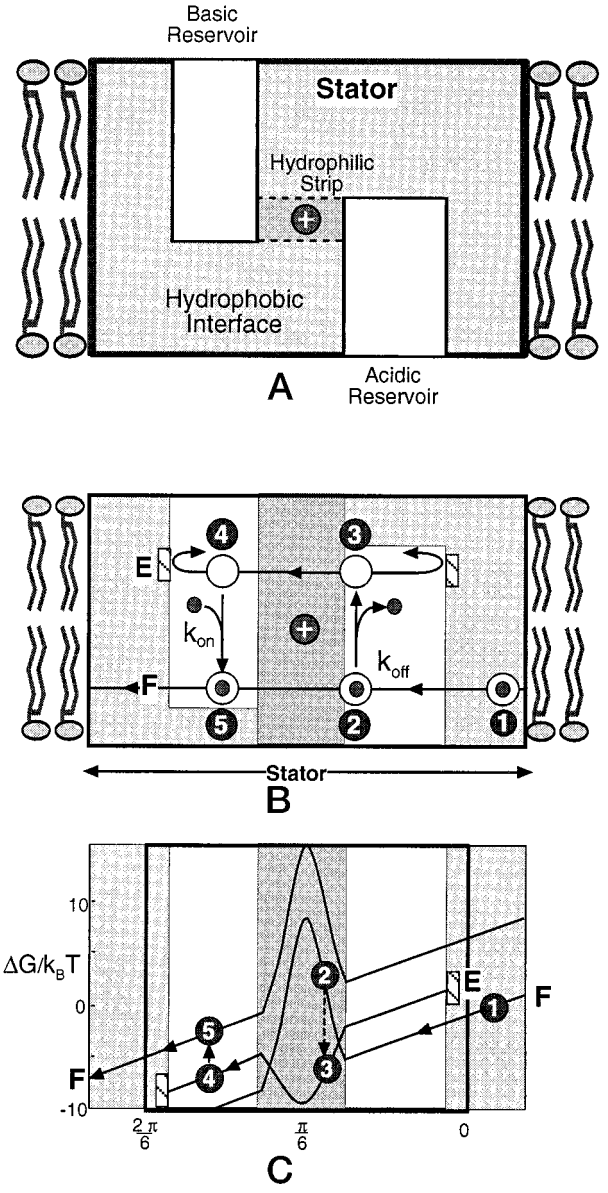

FIGURE 3 (*a*) A face-on cartoon of the stator geometry corresponding to the events in (*b*) and (*c*). (*b*) A typical sequence of events following a site as it passes through the rotor-stator interface. **(1 → 2):** The V_1 motor rotates a protonated site out of the membrane, across the hydrophobic interface, and into the acidic channel. In the channel the site has a high probability of staying protonated since k_{on} is large. However, when the protonated site rotates close to the stator charge, the rotor site pK_a decreases so that k_{off} increases until the proton is relinquished to the acidic reservoir **(2 → 3).** The empty site is then driven through the hydrophilic strip, past the stator charge, and into the basic reservoir **(3 → 4).** An empty site in the basic channel is reflected by the dielectric boundary until a proton binds, neutralizing the site **(4 → 5).** The torque from V_1 can then rotate the site through the hydrophobic barrier (where $k_{off} \sim 0$) into the membrane region. The protonated site continues to rotate one full turn back to position **(1)** where the cycle repeats. (*c*) The free energy of a site as it passes through the rotor-stator interface. The free energy scale corresponds to a rotor site with pK_a = 5.4 pumping from pH = 7 to pH = 4. The potential curve is tilted due to the 45 pN · nm torque from V_1 driving the rotor to the left. **(1 → 2):** the site is driven out of the lipid bilayer into the acidic channel and approaches the stator charge. As the pK_a of the rotor site decreases, the free energy of the site increases until the proton is driven off the site into the acidic channel **(2 → 3). (3 → 4)**: the V_1 motor must supply sufficient torque to pull the rotor site out of the electrostatic grasp of the stator charge and into the basic reservoir. However, it cannot surmount the hydrophobic barrier at the channel boundary. Eventually, the site will protonate **(4 → 5)** whereupon it can be driven through the hydrophobic rotor-stator interface into the membrane domain.

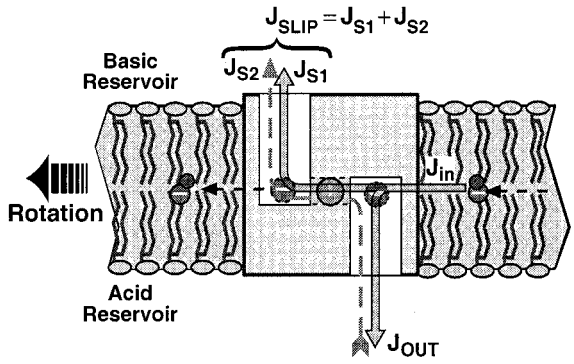

FIGURE 4 The possible pathways for protons passing through the stator. A fraction of the protons that rotate into the output channel "slip" past the stator charge and ride on the rotor site out of the stator, where they dissociate back into the basic reservoir. The proton flux, J_{IN}, enters from the cytoplasmic channel, makes one complete revolution (to the left) and reenters the stator on the right. A fraction, J_{OUT}, dissociates into the output channel, and a fraction J_{S1}, slips past the stator charge and leaves the input channel; thus $J_{S1} = J_{IN} - J_{OUT}$. Actually, a site traversing the output channel will bind and dissociate a proton $\sim 10^4$–10^5 times (see Appendix C), so the proton that "slips" back into the basic reservoir is unlikely to be the same one that initially entered on the rotor site. Additionally, the back-and-forth diffusive motion of the rotor may shuttle protons from the output channel to the basic reservoir, creating a second contribution to the slip flux, J_{S2}. Thus the total slip flux is $J_{SLIP} = J_{S1} + J_{S2}$. This second component of the slip flux is only important when the V_1 motor is nearly at stall, i.e., when the rotation rate of V_o is small.

consumes three ATPs and delivers six protons from the cytoplasm to the lumen. The *coupling ratio*, χ, is defined as the ratio of protons transported per ATP consumed:

$$\chi = J_H/J_{ATP} \tag{3}$$

where J_H is the proton flux and J_{ATP} is the ATP hydrolysis rate. The pH gradient and the membrane potential are thought to affect the value of χ (Davies et al., 1994; Muller et al., 1996). This is generally interpreted as evidence of some sort of "slip" within the pump mechanism. We can formulate this notion within the context of the model as follows.

To define the slip coefficient we first introduce some notation (see Fig. 4):

- J_{In} = flux of protons that enter the stator hydrophobic interface from the basic reservoir (i.e., from the right in Fig. 4);
- J_{Out} = flux of protons that enter the stator hydrophobic interface and successfully dissociate into the output channel;
- J_{S1} = flux of protons that enter the stator hydrophobic interface from the right but pass the stator charge and dissociate back into the basic reservoir. This is part of the slip flux;
- J_{S2} = leak flux of protons shuttled by rotor sites that fluctuate between the output channel and input channel;

- $J_{In} = J_{Out} + J_{S1}$. Since we assume the rotation of V_1 is tightly coupled to ATP hydrolysis, we have $J_{In} = 2 \cdot J_{ATP}$;
- The proton pumping rate is $J_{Out} - J_{S2}$.

With these definitions, the slip coefficient, σ, can be defined as

$$\sigma \equiv 1 - \frac{\text{Pump rate}}{J_{In}} = \frac{J_{S1} + J_{S2}}{J_{In}} \quad (4)$$

The first part of the slip coefficient measures the fraction of protons that enter the stator but do not successfully dissociate into the output channel. J_{S1} is dominant, except near stall, where J_{S2} becomes important. Slip is related to the coupling ratio by:

$$\sigma = 1 - \chi/2. \quad (5)$$

Proton slip is affected by any mechanism that changes the binding or dissociation rates of protons to the rotor site in the proton channels. Increasing the membrane potential or decreasing lumenal pH increases the proton concentration adjacent to the rotor sites facing the output channel, thus increasing the proton binding rate. This increases the probability that a protonated site will rotate out of the output channel carrying a proton into the input channel.

RESULTS

In this section we compute the behavior of the V-ATPase model and compare it to available experimental data. Tables 1 and 2 summarize the parameter values used to calculate the results of this section. We define the membrane potential as $\Delta\Psi = \Psi$ (cytoplasm) $- \Psi$ (lumen) and current flow into the compartment is taken as positive. Therefore, a positive membrane potential will drive positive current flow into the vacuole.

Current-voltage relationships

The basic operating characteristic of an electrogenic ion pump is its current voltage behavior. Such data on V-ATPase proton pumps is scarce, but three sets of data on plant vacuoles by Davies et al. (1994), Bentrup et al. (1986), and Gambale et al. (1994) are presented in Fig. 5. The model fits these data sets well using the parameter values shown in Tables 1 and 2. These three experiments were performed at saturating ATP concentrations where ATP binding was not a rate-limiting step. The load-velocity curve of the V_1 motor used to drive the pump was derived previously, and is discussed in Appendix F (Wang and Oster, 1998).

TABLE 1 Parameters used in all simulations

Parameter	Numerical Value
Screening length ($1/\lambda$)	0.67 nm
Rotational diffusion constant of rotor (D_r)	1.0×10^4 s^{-1}
Proton diffusion constant (D_p)	9.3×10^9 nm^2 s^{-1}
Dielectric constant of cytoplasm (ϵ_c)	80
Dielectric constant of stator (ϵ_s)	4.0
Proton conductivity of lumenal channel	2.2×10^{10} M^{-1} s^{-1}
Proton conductivity of cytoplasmic channel*	2.2×10^{10} M^{-1} s^{-1}
Dipole length of protonated site	0.22 nm
Radius of rotor (R)	3 nm
Bilayer viscosity (η)	10 poise
Zero load rotation rate of V_1	20 Hz

*Except the top panel of Fig. 5, where it is 4.4×10^{10} M^{-1} s^{-1}.

In Appendix J we show that the membrane potential is more effective in resisting the proton flux than the pH gradient (see Fig. 11 *a*). The reason for this is that the membrane potential drop over the polar strip tilts the electrostatic potential seen by the unprotonated site, thus biasing its escape from the central stator charge to the output channel (**2** $\rightarrow$ **3** in Fig. 3 *c*). This escape requires a thermal fluctuation so that the probability of escape depends exponentially on the depth of the well. The imposed membrane potential lowers the height of this barrier in one direction. This strong influence on the dynamics is required to explain why the top two panels of Fig. 5 span two orders of magnitude in the proton pump rate over the range of imposed membrane potentials.

The strength of the electrostatic interaction between the stator and the rotor determines the amount of slip and the overall rotation rate of the enzyme. To compute this interaction involves accounting for the geometry and dielectric environment of the rotor and stator charges. Without a molecular structure this cannot be done realistically, and so we have represented this interaction strength by varying the size of the effective stator charge and the pK_a of the rotor sites. However, there are other contributing factors of equivalent weight that we hold constant, such as the distance between charges, the stator dielectric constant, and the screening length; details of the calculation are given in Appendix D. In general, a large stator charge reduces the rotation and pumping rate. However, if the stator charge is too small the proton flux may prematurely vanish near stall because of increased slip. The top panel in Fig. 5 exhibits this effect: the flux drops to zero long before the thermodynamic stall of ~ -300 mV, because the effective stator charge is too small.

To fit the data in Fig. 5 we must estimate the total number of active pumps. We deduced this by scaling the single pump rate to the observed experimental currents. This scaling parameter affects the height and slope of the current voltage curve. Appendix G describes how the pump densities for each system were determined from fitting the current-voltage curves.

What limits the pH to which the V-ATPase can pump?

Under physiological conditions the free energy of ATP hydrolysis is $\sim 21\ k_BT$, and the energy required to move a proton against a pure concentration gradient is 2.3 ΔpH (in units of k_BT). If six protons are transported across the lumen at the expense of three ATPs, the maximum pH gradient is $6 \times (2.3\ \Delta\text{pH}_{max}) = 3 \times (21\ k_BT)$; thus the thermodynamic

TABLE 2 The parameters that were varied to fit the current-voltage curves (Fig. 5) and illustrate synthesis (Fig. 6)

Parameter	Gambale et al.	Bentrup et al.	Davies et al.	Fig. 6
Pumps/μm^2	480–1900	670	830	—
Central stator charge (elementary charge)	0.5	1.4	1.4	1.4
Rotor pK_a	5.6	5.4	5.4	5.4
Free energy of ATP hydrolysis*	25 k_BT	25 k_BT	25 k_BT	—
Radial position of central stator charge	3.63 nm	3.6 nm	3.6 nm	3.54 nm
Lumenal pH	8	5	5.5	—
Cytoplasmic pH	8	7	8	—

*The ADP, ATP, and P_i levels in these three experiments are not given. Since they are carried out to stimulate hydrolysis (i.e., high ATP concentrations), a large but reasonable free energy for hydrolysis was used in the simulations.

limiting pH gradient attainable is $\Delta pH_{max} = (3 \times 21)/(2.3 \times 6) \sim 4.6$. By comparison, the maximum ΔpH the F-ATPase can achieve when operating in the reverse (pump) direction is $\Delta pH_{max} = (3 \times 21)/(2.3 \times 12) \sim 2.3$. The model provides a way to understand these thermodynamic limits in mechanistic terms.

F_1 is a rotary motor driven by ATP hydrolysis. Under physiological conditions it develops a rotary torque of ~40 pN · nm (Kinosita et al., 1999; Wang and Oster, 1998). F_o is also a rotary motor that is driven in the opposite direction by a transmembrane ion-motive force (Dimroth et al., 1999; Elston et al., 1998). The two motors are connected by a common shaft so that the torque developed by each motor opposes the other. According to the binding change mechanism of Boyer, during ATP synthesis the F_o motor must develop a torque sufficient to free tightly bound ATP from the catalytic site (Boyer, 1997, 1998). That is, it must develop a counter-torque in excess of that developed by the F_1 motor. The mechanochemical theory for the F_o motor is given in Dimroth et al. (1999) and Elston et al. (1998). The important result of this analysis is that the F_o motor operates as a Brownian ratchet wherein the rotational diffusion of the rotor is rectified by the transmembrane proton-motive gradient (Peskin et al., 1993). This means that the F_o motor is a stochastic "stepper" with step size equal to $2\pi R/12$, where $R \sim 3$–4 nm is the rotor radius. The consequence of reducing the number of rotor charges from 12 to 6 is that the rotor is required to diffuse twice as far before being rectified. Since thermal fluctuations are Boltzmann distributed, under the load from V_1 such a fluctuation is exponentially more rare, and so the V_o motor is much less effective than the F_o motor. This gives a greater advantage to the V_1 motor, which can drive the rotor in reverse more effectively, and so the V_o V_1 assembly functions better as a pump; that is, it can achieve lower lumenal pH values, but it will take longer to pump down. Fig. 11 in Appendix J compares the pump performances of the V-ATPase with those of the F-ATPase based on this difference in the number of rotor charges.

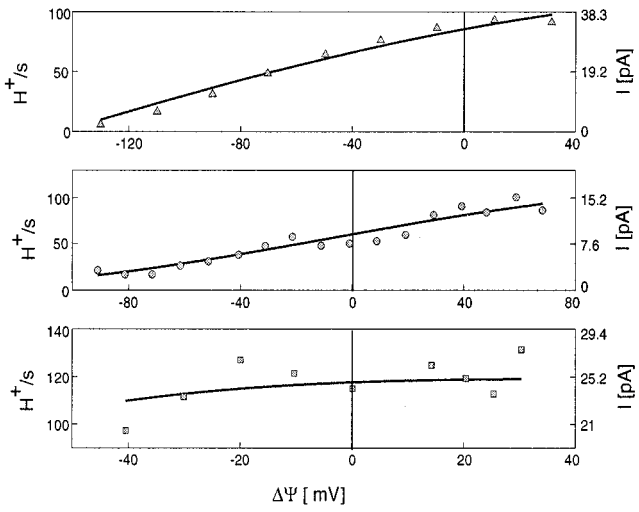

FIGURE 5 V-ATPase current-voltage behavior. The left ordinate is current caused by one pump: protons/s/pump (positive is flow inward). The right ordinate is the total current by all pumps in pA = 0.62×10^7 H^+/s. The abscissa is the imposed transmembrane voltage. The solid lines are computed from the model using the parameters in Tables 1 and 2. The most important parameters in fitting the data were the voltage drop across the polar strip, the effective strength of the stator charge, and the estimated number of pumps (Appendix G). The top panel shows the data (*triangles*) of Gambale *et al.* (1994) on the sugar beet. This is the ATP-dependent current for the enzyme pumping against no pH gradient. The middle panel shows the data (*circles*) of Davies *et al.* (1994) on the red beet (*Beta vulgaris*) pumping from pH 8 (cytoplasm) to pH 5.5 (lumen). The bottom panel shows the ATP-dependent current-voltage values (*squares*) recorded by Bentrup *et al.* (1986) from isolated *Chenopodium rubrum L.* vacuoles when pumping from pH 7 (cytoplasm) to pH 5 (lumen).

Because of the ineffectiveness of the V_o as a motor, one expects that under normal conditions the V-ATPases do not reverse and synthesize ATP: the normal function of the F-ATPases. However, Yokoyama *et al.* (1998) have reported recently that proteoliposomes containing bacteriorhodopsin and the V-ATPase from *Thermus thermophilus* can synthesize ATP when the concentration of Mg-ADP and phosphate is high enough (see Note 2). Fig. 6 shows the range of proton-motive force where the V-ATPase is capable of synthesizing ATP from phosphate and ADP. The curve separating pumping from synthesis in this figure corresponds to the pmf required for the V-ATPase to produce the 45 pN · nm torque required for ATP synthesis. For a tightly coupled system (no slip), this curve can be deter-

mined from thermodynamics without appealing to a dynamic model. However, thermodynamics says nothing about the behavior of the enzyme away from the stall point. Fig. 6 shows that the model predicts that the rotation rate in the synthesis direction quickly increases to a point where ATP production can reach measurable quantities such as those seen in the experiments of Yokoyama *et al.* At physiological values of the vacuolar membrane potential, 10–30 mV, it would require a lumenal pH <2 in order to drive synthesis of ATP (this range of Ψ is not plotted in Fig. 6).

Finally, it is puzzling to find situations in which cells can achieve a pH < 1, since this would appear to violate the above thermodynamic limits (Futai et al., 1998). However, recent structural studies on the F_o rotor suggest a theoretical mechanism. Rastogi and Girvin (1999) demonstrated that the proton binding c-subunit has a different conformation at acidic and basic conditions, with the protonable rotor site (Asp-61) rotating so that the site is buried within the rotor structure at pH $\sim$ 5, but exposed at the rotor periphery at pH $\sim$ 8. This suggests the following scenario for V-ATPases attempting to pump down to very low pH. If exposure to a very acidic lumenal environment titrates rotor sites such that they are withdrawn from participation in proton exchange, then the number of *active* rotor sites could be reduced from six to, say, three. This would make the back torque developed by the V_o motor even smaller in opposing the torque from V_1, and so the pump would pump slower, but be capable of achieving a ΔpH $\sim$ 9, which could account for the phenomenon of such acidic organelles. Of course, some other pump than the V-ATPases may be involved in pumping down to these unusual pH values. However, the ability to sense the lumenal pH is theoretically attractive since it would allow the pump to "change gears" and adapt to a steeper ΔpH, analogous to a bicyclist pedaling up an increasing slope.

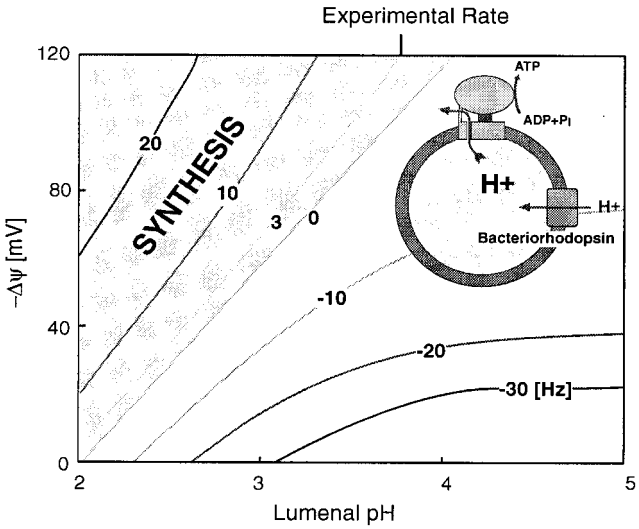

FIGURE 6 ATP synthesis by the V-ATPase. With the cytoplasmic pH fixed at 7, the V-ATPase rotation rate is plotted as a function of lumenal pH and membrane potential. The shaded region corresponds to conditions when the enzyme operates in reverse to synthesize ATP. The experiments of Yokoyama *et al.* (1998) have shown ATP synthesis is possible in light-driven bacteriorhodopsin-V_oV_1-ATPase proteoliposomes. The coupling to V_1 was simulated by providing a constant torque of 45 pN · nm, equivalent to that produced by hydrolyzing three ATPs per revolution (Elston et al., 1998; Wang and Oster, 1998). The approximate number of V-ATPases can be calculated from the amount of purified enzyme used in the experiment. Assuming 100% activity, a lower limit of 6–10 ATP/s per enzyme was calculated as an average synthesis rate over the course of the experiment. This rate corresponds to the 3 Hz curve shown on the figure.

SUMMARY AND DISCUSSION

Because of the lack of structural information, models of ion pumps have necessarily been formulated as kinetic equations describing the proposed chemical steps involved in ion translocation (e.g., Lauger, 1991). This approach omits all mechanical details of how ion translocation actually takes place and how the energy derived from nucleotide hydrolysis is stoichiometrically coupled to translocation. Here we have exploited the close structural similarities between the F and V-ATPases to propose a mechanochemical model of the V-ATPase proton pump. The advantages of this formulation over kinetic models are manifold. First, the model provides a mechanical interpretation of the pump operation that can quantitatively reproduce a variety of experimental observations. Second, by delineating precisely how the energy derived from ATP hydrolysis is used to pump up a transmembrane ion gradient it offers a mechanistic explanation of what is meant by "osmotic work," "slip," and how non-integer coupling ratios arise. Third, the model gives insight into the physics of possible regulatory mechanisms. Finally, the model makes it possible to compute a "pumping surface," like the one pictured in Fig. 7, giving the proton flux as a function of ΔpH and membrane potential. This surface has been partially calibrated by patch clamp studies; however, more thorough experiments must be carried out to construct an accurate pump response to the two components of the proton-motive force. With a reliable pumping surface one can construct a model compartment that incorporates a variety of other proteins that affect lumenal pH, including proton and ion leaks, Donnan potentials, and other electrogenic pumps such as the sodium/potassium ATPase. Such a model could be an important exploratory and explanatory tool for understanding intracellular pH regulation. Since these compartments are not always in thermodynamic equilibrium with each other, a nonequilibrium model is essential (Farinas and Verkman, 1999; Wu et al., 1999). We shall present such a model in a subsequent publication.

The structure of the V-ATPases is not known with the fidelity of the F-ATPases, and so there is more uncertainty about the details of their operation. However, we suggest that the principle of operation we have proposed will find concrete interpretations in the molecular structures that will surely be forthcoming in the near future. Our analysis of the

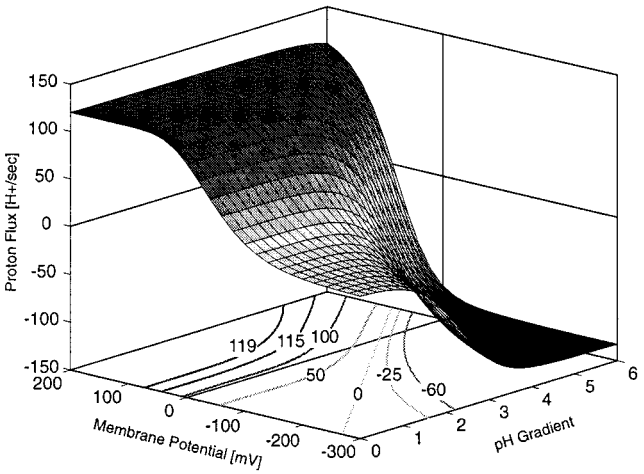

FIGURE 7 The performance surface for a single, tightly coupled V-ATPase. The proton pumping rate is plotted as a function of membrane potential and pH gradient. The cytoplasmic pH is 7 and the free energy of ATP hydrolysis is 21 k_BT. The parameters used are identical to those found in Table 4 for six sites.

rotor-stator interactions reveals that electrostatics plays the central role in regulating proton flow. Finally, we believe that certain aspects of the operating principles governing the V-ATPases will apply in modified form to the P-type ATPase pumps. Both operate on the "alternating access" principle (Alberts et al., 1994; Jencks, 1989) whereby a conformational change moves a tightly bound ion exposed to the basic side of the membrane to a position where it faces the acidic side of the membrane while simultaneously reducing its binding affinity so that it can dissociate. The conformational changes driving translocation in the P-type pumps are not rotations in the plane of the membrane, but are likely to involve small motions perpendicular to the membrane. Moreover, the ATPase driving these motions appears to be more intimately associated with the translocation machinery than they are in the V-ATPases (Scarborough, 1999). However, we believe that the mechanism by which the V-ATPases reduce the ion-binding affinity of the carrier sites by forcing them into proximity to oppositely charged fixed sites will find an analog process in the P-ATPases. Perhaps even the basic mechanisms by which mechanical forces are driven by nucleotide hydrolysis will prove universal (Oster and Wang, 2000; Wang and Oster, 1998).

NOTES

1. The equivalent sequence of events for the one channel model is as follows. Rotor sites are in equilibrium with the basic reservoir. Until a rotor site is protonated, the torque generated by V_1 cannot force it over the hydrophobic barrier. However, once neutralized by protonation, the site is driven across the barrier into the stator output channel. A protonated site that rotates out of the channel into the polar strip interacts electrostatically with the stator charge, which reduces its pK_a, forcing it to relinquish its proton to the acidic reservoir. Further rotation of the rotor carries the rotor site out of the stator interface. After that, the rotor site is once again in equilibrium with the basic reservoir.
2. The proteolipid subunits have a molecular weight of 13 (Yokoyama et al., 1994), comparable to the c-subunits of eucaryotic V-ATPases (~14–16 kDa) consistent with the existence of only six binding sites.

APPENDIX A

Topology of the a-subunit and the rotor-stator assembly

Fig. 8 shows the topology and charge composition of the a-subunit of yeast V-ATPase adapted from Leng et al. (1999). From this arrangement we shall attempt to identify the key structural elements discussed in the section Model Geometry; however, because the evidence is still somewhat controversial, the following observations should be viewed as speculative. Considering the α-helical packing, it is likely that three or four stator helices comprise the rotor-stator interface. We have highlighted several highly polar regions that are likely to form the hydrophilic strip and aqueous channel. None of the identified polar regions spans the entire width of the putative α-helix. The rotor-stator interface must present a hydrophobic barrier against leakage of ions; thus the ion channels should not penetrate all the way through the stator, so that there is no direct path connecting the lumen with the cytoplasm.

It is plausible that the helices in Fig. 8 could form a tertiary structure in which all three charged residues (Lys-593, His-743, and Glu-789) come close to where the rotor charges are hypothesized to pass. For many of our simulations we have used an effective stator charge of +1.4 fundamental charge units at a position radially offset from the rotor by 0.6 nm. This is consistent with two positive and one negative charges electrostatically affecting the rotor sites.

Mutational studies suggest that deletion of the negative residue, Glu-789, drastically reduces enzyme activity (Leng et al., 1996). In the present model, this would make the effective stator charge much larger. In turn, this considerably reduces ATP hydrolysis and proton pumping due to increased rotor-stator electrostatic interactions. In a similar model for F_o operating in the pump direction, it has been shown that it is still possible to transport protons without a central stator charge; however, the experimental range of operation is limited and the overall rate is reduced (Elston et al., 1998). Another possibility is that some of these charges are important for maintaining the structure of the proton channel.

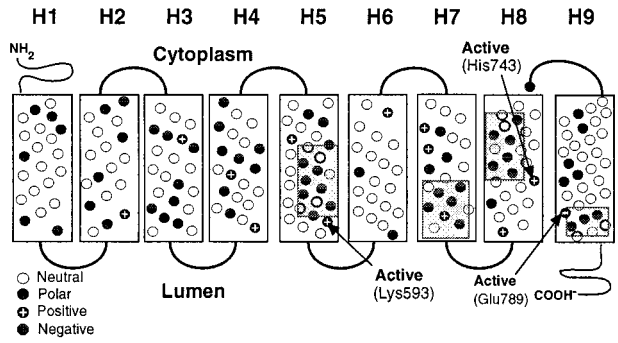

FIGURE 8 A possible topology of the a subunit (Vph1p) showing the polar, charged, and neutral residues. Highlighted areas are highly polar regions that may play the role of the hydrophilic strip discussed in the section Model Geometry.

APPENDIX B

Time evolution of the rotor state

The V-ATPase rotor has six protonatable sites, each of which can be empty (charged) or occupied by a proton (nearly neutral). Thus the state of the rotor at any instant can be specified by $2^6 = 64$ integers. However, force generation takes place near the stator which, in the model, subtends only an angle $2\pi/6$. At most, two sites at a time are interacting with the stator. Therefore, we need track only four rotor sites comprising $2^4 = 16$ chemical states, which we number 1 . . . 16, corresponding to the states (0 0 0 0), (1 0 0 0), . . . , (1 1 1 1). The sequence number, N, of the state (i_1 i_2 i_3 i_4) is given by

$$N = i_1 \times 8 + i_2 \times 4 + i_3 \times 2 + i_4 + 1 \tag{6}$$

Transitions between states occur when a site binds or releases a proton. Since these association/dissociation reactions are much faster than the mechanical motion of the rotor, we can treat the transitions between these states as a Markov chain (Elston et al., 1998). Because of the electrostatic interactions between the rotor sites and the stator charge, the transitions between states depend on the angular position of the rotor, θ. At each angular position and time, the probability of being in any of the $i = 1, \ldots, 16$ states is denoted by $\rho(t; \theta, i)$. The time evolution of this quantity is given by:

$$\frac{\mathrm{d}}{\mathrm{d}t}\begin{bmatrix} \rho(t;\theta,1) \\ \rho(t;\theta,2) \\ \vdots \\ \rho(t;\theta,16) \end{bmatrix} = \mathbf{K}(\theta)\cdot\left.\begin{bmatrix} \rho(t;\theta,1) \\ \rho(t;\theta,2) \\ \vdots \\ \rho(t;\theta,16) \end{bmatrix}\right\} 16 \text{ components} \tag{7}$$

$\mathbf{K}(\theta)$ is a matrix comprised of all the transition rates between states:

$$\mathbf{K}(\theta) = \begin{bmatrix} -\Sigma_1 & k_{2,1}(\theta) & \cdots & k_{15,1}(\theta) & k_{16,1}(\theta) \\ k_{1,2}(\theta) & -\Sigma_2 & \cdots & k_{15,2}(\theta) & k_{16,2}(\theta) \\ \vdots & \vdots & \ddots & \vdots & \vdots \\ k_{1,15}(\theta) & k_{2,15}(\theta) & \cdots & -\Sigma_{15} & k_{16,15}(\theta) \\ k_{1,16}(\theta) & k_{2,16}(\theta) & \cdots & k_{15,16}(\theta) & -\Sigma_{16} \end{bmatrix} \tag{8}$$

$k_{i,j}(\theta)$ is the transition rate from the ith state to the jth state; the diagonal entries are given by sum of all the ways to leave the ith state:

$$\Sigma_i = \sum_j k_{i,j}(\theta) \tag{9}$$

The transition rate $k_{i,j}(\theta)$ is nonzero only when states i and j can be connected by the single event of a proton binding onto or dissociating from a rotor site. For example, the first row of the transition matrix $\mathbf{K}(\theta)$ is:

- $k_{2,1}(\theta)$: transition rate from state 2 = (0 0 0 1) to state 1 = (0 0 0 0);
- $k_{3,1}(\theta)$: transition rate from state 3 = (0 0 1 0) to state 1 = (0 0 0 0);
- $k_{5,1}(\theta)$: transition rate from state 5 = (0 1 0 0) to state 1 = (0 0 0 0);
- $k_{9,1}(\theta)$: transition rate from state 9 = (1 0 0 0) to state 1 = (0 0 0 0).
- $-\Sigma_1 = -(k_{1,2}(\theta) + k_{1,3}(\theta) + k_{1,5}(\theta) + k_{1,9}(\theta))$: all transitions leaving state 1 = (0 0 0 0).

APPENDIX C

Transition rates for the rotor sites

The association rate for an empty rotor site can be determined by computing the time it takes for a proton in the reservoir to diffuse to the site. We use the rate expression corresponding to diffusion to an absorbing boundary to estimate this rate. For the acidic and basic channels, the mouth of the channel is modeled as a disk of radius $r \approx$ 3–5 Å (see Fig. 9). The general

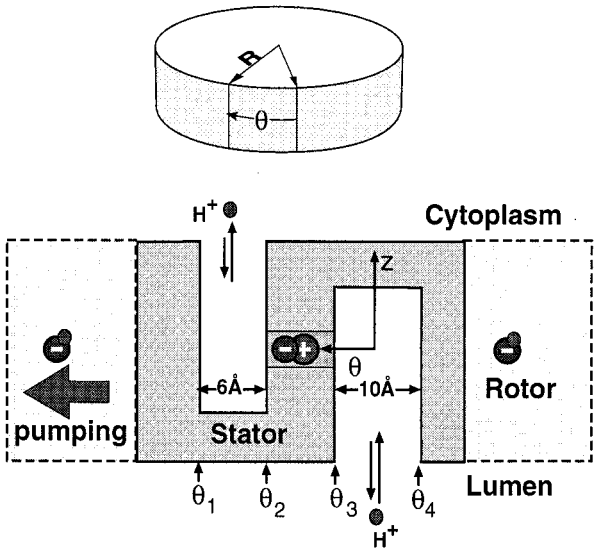

FIGURE 9 The rotor-stator assembly projected onto the rotor surface. The top figure gives a 3D perspective, while the bottom figure is the view from the *outside* of the rotor. The rotation direction for the pump is to the left. If the stator spans four α-helices, then only one rotor site will be in the interface at a time. The acidic and basic channels penetrate the stator to the level of the rotor sites. A hydrophilic strip connects the two channels, allowing unprotonated sites to pass. The stator charge blocks passage of protons through this strip. The approximate size of each channel is given in angstroms.

form of the rate constant is:

$$k_{\mathrm{on}} = \begin{pmatrix} \text{surface proton} \\ \text{concentration} \end{pmatrix} \cdot \begin{pmatrix} \text{flux to a perfectly} \\ \text{absorbing boundary} \end{pmatrix} \tag{10}$$

This is ($10^{-\mathrm{pH}}$ is the proton concentration in mole/liter; 1 mole/liter = 0.6 molecules/nm^3):

$$\begin{aligned} k_{\mathrm{on}}^{\mathrm{Lumen}} &= \underbrace{0.6\ \mathrm{nm}^{-3}\cdot 10^{-\mathrm{pH}_{\mathrm{Lumen}}}}_{\substack{\text{proton concentration} \\ \text{in acidic reservoir}}} \cdot \underbrace{4r_1\cdot D_{\mathrm{p}}}_{\substack{\text{absorption rate} \\ \text{channel entrance}}} \\ k_{\mathrm{on}}^{\mathrm{Cyto}} &= \underbrace{0.6\ \mathrm{nm}^{-3}\cdot 10^{-\mathrm{pH}_{\mathrm{Cyto}}}}_{\substack{\text{proton concentration} \\ \text{in basic reservoir}}} \cdot \underbrace{4r_2\cdot D_{\mathrm{p}}}_{\substack{\text{absorption rate} \\ \text{channel entrance}}} \end{aligned} \tag{11}$$

Here D_{p} is the diffusion coefficient of a proton in solution and r_1 and r_2 are the equivalent radii of the acidic and basic channel entrances, respectively. The actual rates depend heavily on the surrounding charge geometry and other complicating factors. Therefore, we model the conductivity of a channel by the conductance:

$$g \sim 0.6\ \mathrm{nm}^{-3}\cdot r_{1,2}\cdot D_{\mathrm{p}} \tag{12}$$

The binding rate then becomes:

$$k_{\mathrm{on}} = g\cdot 10^{-\mathrm{pH}} \tag{13}$$

where g has a different value for sites facing the lumenal channel than for those facing the cytoplasmic channel.

The dissociation rate can be calculated from the association rate by enforcing detailed balance and using the definition of pK_{a}. The reaction on

the rotor sites is represented by

$$\text{Glu-140}^- + \text{H}^+ \underset{k_{off}}{\overset{k_{on}}{\rightleftharpoons}} \text{Glu-140} \cdot \text{H}$$

At equilibrium,

$$k_{on} \cdot [\text{Glu-140}^-] = k_{off} \cdot [\text{Glu-140} \cdot \text{H}] \tag{14}$$

From the definition of pK_a, $\text{p}K_a = \text{pH} + \log_{10} \frac{[\text{Glu-140} \cdot \text{H}]}{[\text{Glu-140}^-]}$, we have

$$\frac{[\text{Glu-140} \cdot \text{H}]}{[\text{Glu-140}^-]} = 10^{\text{p}K_a - \text{pH}} \tag{15}$$

The proton dissociation rate, k_{off}, is related to pK_a and k_{on} by combining Eqs. 14 and 15:

$$k_{off} = k_{on} \cdot 10^{\text{pH}-\text{p}K_a} = g \cdot 10^{-\text{p}K_a} \tag{16}$$

The mean time for dissociation and rebinding of a proton with the rotor site is $(k_{on} + k_{off})/(k_{on} \cdot k_{off})$. Using a p$K_a$ of 5.4 and a lumenal pH of 5, this time is $\sim 10^{-5}$ s. At a rotation rate of 20 Hz, it takes $\sim$0.02 s for a rotor site to traverse the acidic channel. This means that, on average, the proton visits the site $0.02/10^{-5} = 2{,}000$ times during the period when the site is facing the acidic channel.

Finally, the central stator charge and the electrical potential across the aqueous channel will shift the equilibrium distribution of the ionized and unionized states. A Boltzmann factor with the appropriate energetic differences between the on and off states modifies the previous off rate to give the distribution

$$\begin{aligned} k_{i,j}^{off}(\theta) &= k_{off} \cdot \exp\left(\frac{\Delta\phi_{i,j}^{Q} + \Delta\phi_{i,j}^{\Psi}}{k_B T}\right) \\ \Delta\phi_{i,j}^{Q} &\equiv \phi_Q(\theta, i) - \phi_Q(\theta, j) \\ \Delta\phi_{i,j}^{\Psi} &\equiv \phi_\Psi(\theta, i) - \phi_\Psi(\theta, j) \end{aligned} \tag{17}$$

where $\Delta\phi_{i,j}^{Q}$ is the difference in energy for moving a proton from the bulk solution to the rotor site in the electrostatic field of the stator charge and $\Delta\phi_{i,j}^{\Psi}$ is the energy of moving the proton in the electric field caused by the membrane potential. Both of these differences are calculated by using Eqs. 23 and 24, respectively, to find the corresponding energy of states *i* and *j*. When a site is in the hydrophobic interface it is not allowed to exchange with the lumen or the cytoplasm, so the rates are set to zero in this angular interval.

APPENDIX D

The interaction between the rotor and stator

We erect a cylindrical coordinate system on the rotor-stator assembly as shown in Fig. 9. The *z*-axis passes through the center of the rotor and is perpendicular to the plane formed by the six binding sites. We set $z = 0$ at the level of the binding sites. The radial distance, *r*, from the *z*-axis to the binding sites is taken to be 3 nm. When the protons bind to this site, they do so at a fixed distance of 0.22 nm radially outward from the binding site:

$$\begin{aligned} r_{site} &= 3.0 \text{ nm}; \quad & z_{site} &= 0.0 \text{ nm} \\ r_{proton} &= 3.22 \text{ nm}; \quad & z_{proton} &= 0.0 \text{ nm} \end{aligned} \tag{18}$$

We take the angular distance between the rotor sites as the unit of displacement: $\Delta\theta = 2\pi/6$. Using this notation, we specify the stator arrangement used for all calculations (see Fig. 9)

$$\begin{aligned} \theta_1 &= +0.35 \times \Delta\theta \\ \theta_2 &= +0.125 \times \Delta\theta \\ \theta_3 &= -0.125 \times \Delta\theta \\ \theta_4 &= -0.5 \times \Delta\theta \end{aligned} \tag{19}$$

Finally, we model the electrostatic effect of the charged trio Lys-593, His-743, and Glu-789 by an equivalent charge, denoted *Q*, located at

$$\theta_Q = 0.0; \quad r_Q = 3.54 \text{ nm}; \quad z_Q = 0.0 \text{ nm} \tag{20}$$

The electrostatic interactions between the rotor site and the stator determine the rotor dynamics. Since everything occurs at the $z = 0$ level, we ignore this coordinate. The hydrophobic interface lies in the region $\theta \geq \theta_1$ and the region $\theta_4 \geq \theta$, and acts as a reflecting boundary for unprotonated sites. In the absence of the stator charge, unprotonated sites can rotate freely across the polar strip. The total electrostatic interaction between the rotor and stator consists of three components:

- $\phi_{\Delta\epsilon}(\theta, \mathbf{s})$ = the interaction caused by the dielectric barrier opposing the entry of a charged site into the hydrophobic rotor-stator interface;
- $\phi_{\Delta\Psi}(\theta, \mathbf{s})$ = the interaction caused by the membrane potential drop across the horizontal hydrophilic strip;
- $\phi_Q(\theta, \mathbf{s})$ = the electrostatic interaction between the rotor charges and the central stator charge, *Q*.

These potentials are computed as follows. A charged site attempting to rotate out of the aqueous environment (with dielectric constant $\epsilon_w \approx 80$) into the hydrophobic interface ($\epsilon_s \approx 4$) encounters an energetic barrier. This energy penalty arises from stripping away the hydration shell of polarized water molecules from the charged site so that it can move into the neutral interface region. However, there is but a small energy barrier facing unprotonated sites that rotate from the aqueous channel into the hydrophilic strip, for they encounter a layer of dipole amino acids along this region that compensates for the loss of the hydration shell. We model the dielectric barrier on a charged (empty) rotor site by:

$$\phi_{\Delta\epsilon}(\theta) = \begin{cases} 200\, k_B T \cdot \Delta(1/\epsilon) \approx 45\, k_B T & \text{if} \quad \theta \geq \theta_1 \quad \text{or} \quad \theta \leq \theta_4 \\ 0 & \text{otherwise} \end{cases} \tag{21}$$

where $\Delta(1/\epsilon)$ is the difference in dielectric constants entering the hydrophobic rotor-stator interface (Israelachvili, 1992). $\phi_{\Delta\epsilon}(\theta, \mathbf{s})$, is calculated by summing up the contributions from the charged (empty) rotor sites near the rotor-stator interface. The electrostatic interactions are calculated using a screened Coulomb potential to simulate the protein interior:

$$\begin{aligned} d(\theta, r) &= \sqrt{[r\cos(\theta) - r_Q \cos(\theta_Q)]^2 + [r\sin(\theta) - r_Q \sin(\theta_Q)]^2} \\ \tilde{\phi}(\theta, r) &= \frac{q}{4\pi\epsilon_0} \cdot \frac{Q}{\epsilon_S d} \cdot \exp(-\lambda d) \end{aligned} \tag{22}$$

where *d* is the distance between the interacting charges, *q* and *Q*, (r, θ) is the position of the charge *q*, and (r_Q, θ_Q) is the position of the stator charge *Q*. The dielectric constant of the rotor-stator interface is $\epsilon_S = 4$, and the Debye screening length is $1/\lambda = 0.67$ nm. Since the radius of the rotor sites is fixed, *r* can be eliminated from the total electrostatic potential. The water in the output channel will raise the dielectric constant substantially over that of the hydrophilic strip. Therefore, the electrostatic interaction be-

tween the stator charge and charges in the channel and the cytoplasm will be small. This leads us to model the field as:

$$\phi_Q(\theta) = \begin{cases} \tilde{\phi}(\theta) - \tilde{\phi}(\theta_2) & \text{if} \quad \theta_3 \le \theta \le \theta_2 \\ 0 & \text{otherwise} \end{cases} \tag{23}$$

$\phi_Q(\theta, \mathbf{s})$ is calculated by summing the contributions from the four rotor binding sites nearest the rotor-stator interface and the contributions from the protons bound on them, if any.

Determining the electric field profile across membrane channels is a complicated calculation that involves solving the Poisson-Boltzmann equation with irregular boundary conditions arising from the protein medium. We use a first-order approximation for the field that assumes a linear profile across the polar strip at the level of the rotor sites. The aqueous channels are assumed to be in equilibrium with the bulk, thus the charge separation of the ions generating the membrane potential occurs across this strip. At the level of the rotor binding sites, the potential due to the transmembrane potential drop is given by (see Fig. 9)

$$\phi_{\Delta\Psi}(\theta) = \begin{cases} \Delta\Psi_{\text{mem}} & \text{if} \quad \theta_2 \le \theta \le \theta_1 \\ \Delta\Psi_{\text{mem}} \cdot (\theta - \theta_3)/(\theta_2 - \theta_3) & \text{if} \quad \theta_3 \le \theta \le \theta_2 \\ 0 & \text{if} \quad \theta_4 \le \theta \le \theta_3 \end{cases} \tag{24}$$

$\phi_{\Delta\Psi}(\theta, \mathbf{s})$ is calculated by summing the contributions from the charged (empty) rotor sites near the rotor-stator interface. If the actual width of the aqueous channel that is accessible to ions decreases, a potential will form along the z-axis between the lipid surface and the rotor site. A more general description involves splitting the potential drop into horizontal and vertical portions:

$$\Delta\Psi = \underbrace{(1 - f) \cdot \Delta\Psi}_{\substack{\text{potential drop across} \\ \text{aqueous channel}}} + \underbrace{f \cdot \Delta\Psi}_{\substack{\text{potential drop across} \\ \text{polar strip}}} \tag{25}$$

Here f is the fraction of the total potential drop, $\Delta\Psi$, across the polar strip.

The sum of all of the potential energies for each state $\mathbf{s}$ is $\mathbf{\Phi}(\theta, \mathbf{s}) = \phi_{\Delta\epsilon}(\theta, \mathbf{s}) + \phi_{\Delta\Psi}(\theta, \mathbf{s}) + \phi_Q(\theta, \mathbf{s})$, which determines the electrostatic contribution to the rotation of the rotor according to Eq. 2.

APPENDIX E

The Fokker-Planck equation for the rotor dynamics

To describe the average mechanical properties of the pump we recast the mechanical Eq. 2 into the Fokker-Planck representation for the probability density of finding the rotor at angular position θ at time t. Thus the equation of motion for $\rho(\theta, t)$ is (Risken, 1989):

$$\frac{\partial \rho}{\partial t} = \underbrace{\frac{1}{\zeta}\frac{\partial}{\partial \theta}(\mathbf{\Phi}'\rho)}_{\substack{\text{Forces between} \\ \text{rotor and stator} \\ \tau_Q,\ \tau_{\Delta\Psi},\ \text{and}\ \tau_{\Delta\epsilon}}} + \underbrace{\frac{1}{\zeta}\frac{\partial}{\partial \theta}(\tau_L(\theta)\rho)}_{\substack{\text{Driving Torque,} \\ \tau_D(\theta)}} + \underbrace{D\frac{\partial^2 \rho}{\partial \theta^2}}_{\substack{\text{Brownian} \\ \text{motion}}} + \underbrace{\mathbf{K}(\theta)\rho}_{\substack{\text{Transitions} \\ \text{between} \\ \text{rotor states}}} \tag{26}$$

Here $\rho(\theta, t)$ is the probability density for the 16 chemical states as a function of position and time and $D = k_B T/\zeta$ is the rotor diffusion coefficient computed from the drag coefficient, ζ, of the cylindrical rotor.

The potential $\Phi(\theta)$ is given by the diagonal matrix

$$\mathbf{\Phi}(\theta) = \left.\begin{bmatrix} \Phi(\theta, 1) & & & & \\ & \Phi(\theta, 2) & & & \\ & & \ddots & & \\ & & & \Phi(\theta, 15) & \\ & & & & \Phi(\theta, 16) \end{bmatrix}\right\} \text{16 rows}$$

$$\underbrace{\qquad\qquad\qquad\qquad}_{\text{16 columns}}$$

where $\Phi(\theta, i)$ is the ith diagonal element of $\mathbf{\Phi}(\theta)$ giving the electrostatic potential between the rotor and the stator corresponding to the ith chemical state.

The steady-state distribution can be found by solving Eq. 26 when $\partial\rho/\partial t = 0$. All average properties of the pump, such as rotation rate and proton flux, can be determined with this probability distribution. Solution of the model equations was performed in Matlab by a finite difference scheme described in Elston et al., (1998). The code is available from the authors on request.

APPENDIX F

Torque generation in V_1

The V_o portion of the pump is driven by torque generated in V_1 by ATP hydrolysis. We model the driving torque using the analysis of the F_1-ATPase given in Noji et al., (1997); Oster and Wang, (2000); Wang and Oster, (1998); and Yasuda et al., (1998). We shall make the following assumptions:

- The rotation of the shaft driving V_o (the D and E subunits) is tightly coupled to the hydrolysis of ATP; that is, three ATPs are consumed per revolution. Therefore, the energy per revolution is $3 \cdot \Delta G_{ATP}$;
- The shaft proteins are flexible so that the torque, τ_D, delivered to V_o is approximately constant (Oster and Wang, 2000). The energy transferred per revolution is $2\pi\ \tau_D$;
- The energy dissipated by V_1 is $2\pi\zeta\omega$, where ω is the average rotation rate [1/s] and ζ is the effective drag coefficient of the rotor.

We shall use an analytic form for the load velocity curve that closely matches that computed using the model developed in Wang and Oster, (1998):

$$\omega(\tau) = \omega(0) \cdot \left(1 - \left(\frac{\tau}{\tau_{\text{stall}}}\right)^6\right) \tag{28}$$

where the $\omega(0) \sim 20$ Hz is the angular velocity at zero load, in accord with the experimental observations of F-ATPase during hydrolysis (Noji et al., 1997; Yasuda et al., 1998). The torque required to stall the V_1 motor is $\tau_{\text{stall}} = (3 \cdot \Delta G_{ATP}/2\pi)$, given by thermodynamic considerations to be ~ 45 pN $\cdot$ nm.

From Fig. 10 we see that this form closely fits the load velocity curve at high ATP concentrations computed using the model developed in Wang and Oster, 1998). It turns out that the shapes of the current voltage curves computed by the model are insensitive to the exact shape of the load velocity curve so long as it is concave down and has the same maximum velocity and stall torque.

APPENDIX G

Calculation of pump densities for Fig. 5

We assume that the pumps work independently under the same physiological conditions. Therefore, the capacity of one pump can be scaled to find

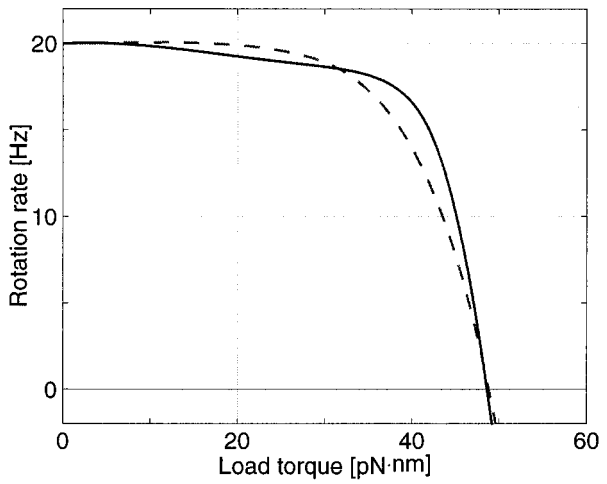

FIGURE 10 The behavior of the pump is not sensitive to the precise form of the load velocity curve, so long as it is concave downward. Therefore, we used an analytical approximation (Eq. 28; *dashed line*) to the load velocity curve computed by Wang and Oster (1998) for F_1 (*solid line*) using the same free energy of ATP hydrolysis (24 k_BT).

the total current across the membrane:

$$I = N \cdot J_P = \rho A J_P \tag{29}$$

where N is the total number of active pumps on the surface, ρ is the pump density, A is the surface area, and J_P is the proton flux due to one pump. Table 3 lists the vacuolar radii for each data set and the corresponding surface area, assuming a spherical geometry (Bentrup et al., 1986; Davies et al., 1994; Gambale et al., 1994). J_p is computed from the model, and A and I are experimentally measured quantities. By scaling our single pump current to the total measured current, we can obtain an estimate of the total number of pumps present in the membrane. Using this, we can infer the pump density for each trial, as given in Table 3. In these calculations it is more convenient to express the current in terms of protons per second rather than picoAmps [pA] because it gives an idea of the number of protons being transported by one pump:

$$1\left[\frac{H^+}{s}\right] \cdot \frac{[\text{coloumb}]}{6.2 \times 10^{18}[H^+]} \cdot \frac{[\text{pA}]}{10^{-12}[A]} = 1.6 \times 10^{-7}[\text{pA}] \tag{30}$$

APPENDIX H

Estimate of the ATP synthesis rate

Here we estimate the average ATP production rate over the first 40 min of the experiment of Yokoyama et al. (1998). After this time, ~25 μmol of ATP have been synthesized per mg of V-ATPase. The V-ATPase protein is ~760 kDa. Therefore, 1 mg of enzyme is:

$$1[\text{mg } V_{ATP}] = \frac{1[\text{Da}]}{1.67 \times 10^{-21}[\text{mg}]} \cdot \frac{1[V_{ATP}]}{760{,}000\,[\text{Da}]} \cdot \frac{1[\text{mol}]}{6.02 \times 10^{23}[\text{mol}]} = 1.3 \times 10^{-9}[\text{mol } V_{ATP}] \tag{31}$$

25 μmol of ATP are synthesized after 2400 s. Thus

$$\text{Synthesis Rate} = \frac{25 \times 10^{-6}[\text{mol ATP}]}{2400\,[\text{s}]} \cdot \frac{1}{1.3 \times 10^{-9}[V_{ATP}]} = 8\left[\frac{\text{ATP}}{\text{s}}\right] \tag{32}$$

This gives about *three revolutions per second* for a single V-ATPase synthesizing ATP. This sets a lower limit on the rotation rate since we have assumed that all pumps are operating. For the conditions under which the experiment was carried out there is good evidence to believe nearly 100% of the enzyme was incorporated into the proteoliposome (K. Yokoyama, personal communication).

TABLE 3 The vacuole radii are experimentally measured, and from scaling our single pump current-voltage curve to the experimentally measured whole vacuole current we are able to estimate the pump density

Parameter	Radii (μm)	Area (μm^2)	Pumps/μm^2
Gambale et al.	20–40	1250–5025	480–1900
Bentrup et al.	25	1950	670
Davies et al.	15	706	830

APPENDIX I

Slip, coupling ratio, and efficiency

The relationship between proton pumping and energy consumption in the V-ATPases is usually expressed as the "coupling ratio," defined as the number of protons transported across the membrane per ATP consumed by the V_1 subunit. In terms of rates,

$$\chi \equiv \frac{J_p}{J_{ATP}} \tag{33}$$

where J_p [protons pumped/s] is the pumping rate of one pump and J_{ATP} [ATP hydrolyzed/s] is the hydrolysis rate of one V-ATPase. We can express this in terms of measurable quantities by defining the related notion of proton "slip" as follows. The proton balance on a vesicle is:

$$\underset{\text{accumulation rate}}{\dot{H}(t)\ \text{Proton}} = \underset{\text{influx}}{J_{net}\ \text{Net proton}} = \underset{\text{pump rate}}{(1-\sigma)NJ_p^*\ \text{Net proton}} - \underset{\text{leak rate}}{J_L\ \text{Net proton}} \tag{34}$$

where $\dot{H} = dH/dt$ is the rate of proton increase in the vesicle, N is the total number of pumps, J_L is the leakage rate through parallel channels (which may be through the pump itself, e.g., leakage past the rotor-stator hydrophobic seal), and J_p^* is the rate of a perfectly coupled pump. By definition, the "slip" coefficient is the ratio of slip rate (the difference between the perfect pump rate and the actual pump rate) to the perfect pump rate. As shown in Fig. 4, the slip flux has two components. The first component (J_{S1}) is the flux of protons that enter the stator hydrophobic interface but do not successfully dissociate into the output channel. These protons ride on the rotor through the stator polar strip and dissociate back into the basic reservoir. The second component (J_{S2}) is the leak flux of protons shuttled by the rotor sites that fluctuate between the output channel and the basic reservoir (cf. Fig. 4).

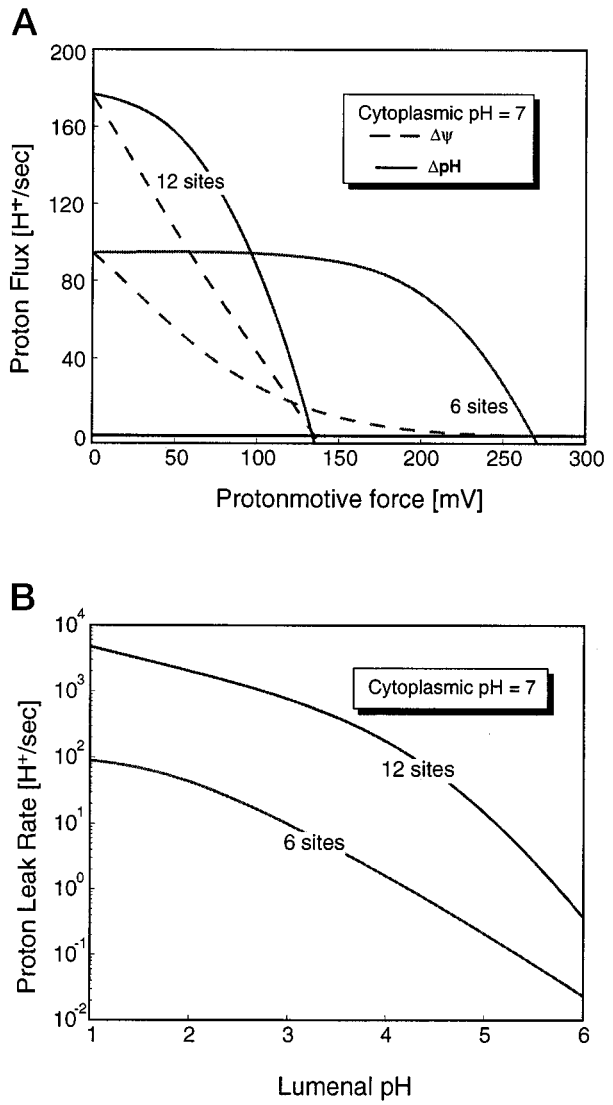

FIGURE 11 Comparison of V and F-ATPase. (*a*) The solid lines show the pump performance when the proton-motive force is a transmembrane ΔpH. With six rotor sites the V-ATPase can pump to a much lower pH, but its maximum pumping rate is lower. The dashed lines show the pump performance when the proton-motive force is exclusively a membrane potential. In this case, the V-ATPase performance drops precipitously as membrane potential increases. (*b*) The leak flux through V_o and F_o when the ATP concentration is zero. Over a large ΔpH, the leakage rate through the pump is almost two orders of magnitude smaller with 6 rotor sites (V_o) than with 12 rotor sites (F_o). Parameter values can be found in Table 4.

TABLE 4 The parameters used to generate Fig. 11 (all other parameters can be found in Table 1)

Parameter	6 Sites	12 Sites
Central stator charge (elementary charge)	1.4	1.4
Diffusion constant of rotor (D_r)	1.0×10^4 s^{-1}	1.0×10^4 s^{-1}
Rotor pK_a	5.4	5.4
Free energy of ATP hydrolysis	21 k_BT	21 k_BT
Radial position of central stator charge	3.54 nm	3.54 nm
Lumenal pH	variable	variable
Cytoplasmic pH	7	7

The slip coefficient, σ, depends upon lumenal and cytoplasmic pH as well as the membrane potential and the presence of negative charges in the output channel that compete with the rotor site for protons (see the discussion on pH regulation) (Davies et al., 1994; Schmidt and Briskin, 1993). Since there is some ambiguity in the literature about what the slip represents and how it is related to the efficiency of the pump, it is useful to define these two quantities precisely in the context of our mechanochemical model for the V-ATPase mechanism.

The work of Noji *et al.* on F_1 demonstrates that *ATP hydrolysis is tightly coupled to the rotation of the γ shaft connecting F_1 to F_0. Moreover, each revolution of the rotor requires the hydrolysis of three ATPs* (Noji et al., 1997; Yasuda et al., 1997, 1998). (The mechanism underlying these observations is explained in Wang and Oster, 1998.) Thus when coupling is perfect ($\sigma = 0$), six protons will be transported across the membrane at the expense of three ATP: $J_p^* = 2J_{ATP}$. Thus Eq. 34 becomes

$$\dot{H}(t) = 2(1 - \sigma)NJ_{ATP-J_L} \tag{35}$$

Experimentally, one can measure the total hydrolysis rate by all pumps, $J_{ATP} = N \cdot J_{ATP}$, and $H(t)$, or a variable monotonic with it. Usually, the initial rate, $\dot{H}(0)$, is measured, from which the slip and coupling ratio are expressed as:

$$\sigma = 1 - \frac{\chi}{2} = 1 - \frac{\dot{H}(0) + J_L}{2 \cdot J_{ATP}} \tag{36}$$

The above equation is only useful in determining the slip (and the coupling ratio) if either the proton leak or the pumping rate can be determined independently of the total proton flux.

The efficiency, η, of the pump is defined as

$$\eta \equiv \frac{\text{Power output as proton transport}}{\text{Power input as ATP hydrolysis}} \tag{37}$$

If the system is in equilibrium both inside and outside the vesicle, the free energy of transport (chemical potential per mole) is given by the proton-motive force, i.e., the free energy to move a proton across the membrane:

$$\Delta G_p = \Delta\Psi - 2.3\left(\frac{RT}{F}\right)\Delta\text{pH} \tag{38}$$

where $\Delta\Psi$ is the membrane potential, R is the gas constant, F is Faraday's constant, and T is the absolute temperature. Denote by ΔG_{ATP} the free energy of hydrolysis of a single ATP (under physiological conditions $\Delta G_{ATP} \sim 12$ kcal/mol $= 20\ k_BT$). Then we can express the pump efficiency as:

$$\eta = \chi \cdot \frac{\Delta G_p}{\Delta G_{ATP}} \tag{39}$$

APPENDIX J

Comparisons between V-ATPase and F-ATPase pump and leak rates

Because of their structural and functional similarities, the F- and V-ATPases probably evolved from a common ancestor (Kibak et al., 1992; Nelson, 1992; Taiz and Nelson, 1996). A major structural difference between the F_o and V_o sectors is that V_o has six c-subunits, each consisting of four transmembrane α-helices, one of which contains the protonable site. In contrast, F_o has 12 c-subunits, each consisting of 2 transmembrane

α-helices. Helix 2 contains the protonable site. Thus the V_o rotor has half the number of proton carriers as F_o. This structural difference strongly influences the pumping capacity, as we now show.

The coupling ratio for the pump, χ, is defined in Eq. 33 as the proton flux divided by the hydrolysis rate. The highest possible coupling ratio for V-ATPase is $\chi_{max} = 2$ protons/ATP, while for F-ATPase, $\chi_{max} = 4$ protons/ATP. From the viewpoint of the model, we can understand two general features that distinguish the V- and F-ATPases.

V-ATPases can pump to lower pH than F-ATPases. Bacterial F-ATPases synthesize ATP under aerobic conditions, but reverse to pump protons under anaerobic conditions. Equilibrium thermodynamics suggests that the V-ATPase, with 6 rotor sites, should be able to pump to a lower pH than F-ATPase, with 12 rotor sites. Hydrolysis of one ATP under cellular conditions yields a free energy of $\sim 21\ k_BT$. Since V_1 consumes three ATPs per revolution, and if rotation is tightly coupled to proton translocation, then the maximum chemical potential achievable by pumping is: $6 \cdot \Delta\mu(V_1) = 3 \cdot \Delta G_{ATP} = 12 \cdot \Delta\mu(F_1)$. Thus $\Delta\mu(F_1)/\Delta\mu(V_1) \sim \frac{1}{2}$. However, since pumping takes place far from equilibrium, the actual relative performance has to be computed at the steady state. Fig. 11 *a* shows a comparison of the computed pumping rate as a function of membrane potential and ΔpH for the V-ATPase and F-ATPase. We see that the V-ATPase can pump against a much higher proton-motive force than the F-ATPase, although its maximum rate is lower.

V-ATPases leak much less than F-ATPases. When the V_1 sector is removed, the permeability of the V_o sector does not change (Beltrán, 1992). In contrast, removal of F_1 results in a considerable increase in proton permeability. Similarly, deprived of ATP, the V-ATPases do not leak protons, while the F-ATPases do. In Fig. 11 *b* we plot the leakage rate for the V-ATPase model with 6 rotor sites compared with the identical configuration with 12 rotor sites. We see that simply halving the number of rotor sites reduces the leakage rate by almost two orders of magnitude over all pH ranges. The reason for this has to do with the diffusive motion of the rotor in the absence of a driving torque from V_1. This diffusive motion is opposed by the potential barriers presented by V_1. In the absence of ATP the V-ATPase rotor must diffuse against this barrier by an angular distance of $2\pi/6$ to shuttle a proton between the acidic and basic compartments, whereas the F-ATPase rotor must diffuse by only $2\pi/12$ (Table 4).

In the absence of a resisting load (i.e., upon removal of the F_1 or V_1 headpiece), the leakage rates in Fig. 11 *b* are much higher, and the difference between the 12 and 6 site curves narrows to a factor of 2 (data not shown). This is counter to the experimental observations noted above. A possible explanation is that one of the many subunits found in V-ATPase, yet absent in F-ATPase, acts as a "brake" on the rotor.

The authors thank Xing-Hong Leng and Lincoln Taiz for valuable assistance during the course of this work, and especially Barry Bowman for his advice with regard to the subunit biochemistry and structural interpretation. In addition, the thoughtful comments of the reviewers have greatly improved the manuscript.

This work was supported by National Science Foundation Grant DMS 9220719.

REFERENCES

Abrahams, J., A. Leslie, R. Lutter, and J. Walker. 1994. Structure at 2.8 Å resolution of F_1-ATPase from bovine heart mitochondria. *Nature.* 370: 621–628.

Alberts, B., D. Bray, J. Lewis, M. Raff, K. Roberts, and J. Watson. 1994. *Molecular Biology of the Cell.* Garland, New York.

Arai, H., G. Terres, S. Pink, and M. Forgac. 1988. Topography and subunit stoichiometry of the coated vesicle proton pump. *J. Biol. Chem.* 263: 8796–8802.

Beltrán, C., and N. Nelson. 1992. The membrane sector of vacuolar H(+)-ATPase by itself is impermeable to protons. *Acta Physiol. Scand. Suppl.* 607:41–47.

Bentrup, F., M. Gogarten-Boekels, B. Hoffmann, J. Gogarten, and C. Baumann. 1986. ATP-dependent acidification and tonoplast hyperpolarization in isolated vacuoles from green suspension cells of *Chenopodium rubrum L. Proc. Natl. Acad. Sci. USA.* 83:2431–2433.

Boekema, E., T. Ubbink-Kok, J. Lolkema, A. Brisson, and W. Konings. 1997. Visualization of a peripheral stalk in V-type ATPase: evidence for the stator structure essential to rotational catalysis. *Proc. Natl. Acad. Sci. USA.* 94:14291–14293.

Boekema, E. J., J. F. L. v. Breemen, A. Brisson, T. Ubbink-Kok, W. N. Konings, and J. S. Lolkema. 1999. Connecting stalks in V-type ATPase. *Nature.* 401:37–38.

Bowman, B., R. Allen, M. Wechser, and E. Bowman. 1988a. Isolation of genes encoding the Neurospora vacuolar ATPase—analysis of vma-2 encoding the 57-kDa polypeptide and comparison to vma-1. *J. Biol. Chem.* 263:14002–14007.

Bowman, E., K. Tenney, and B. Bowman. 1988b. Isolation of genes encoding the Neurospora vacuolar ATPase—analysis of vma-1 encoding the 67-kDa subunit reveals homology to other ATPases. *J. Biol. Chem.* 263:13994–14001.

Boyer, P. 1997. The ATP synthase—a splendid molecular machine. *Annu. Rev. Biochem.* 66:717–749.

Boyer, P. 1998. Energy, life, and ATP (Nobel lecture). *Angew. Chem. Int. Ed.* 37:2296–2307.

Cross, R., and L. Taiz. 1990. Gene duplication as a means for altering H+/ATP ratios during the evolution of F_0F_1 ATPases and synthases. *FEBS Lett.* 259:227–229.

Davies, J. M., I. Hunt, and D. Sanders. 1994. Vacuolar H^+-pumping ATPase variable transport coupling ratio controlled by pH. *Proc. Natl. Acad. Sci. USA.* 91:8547–8551.

Dimroth, P., H. Wang, M. Grabe, and G. Oster. 1999. Energy transduction in the sodium F-ATPase of *Propionigenium modestum. Proc. Natl. Acad. Sci. USA.* 96:4924–4929.

Dmitriev, O. Y., K. Altendorf, and R. H. Fillingame. 1995. Reconstitution of the F-o complex of *Escherichia coli* ATP synthase from isolated subunits: varying the number of essential carboxylates by co-incorporation of wild-type and mutant subunit c after purification in organic solvent. *Eur. J. Biochem.* 233:478–483.

Eisenberg, E., and T. Hill. 1985. Muscle contraction and free energy transduction in biological systems. *Science.* 227:999–1006.

Elston, T., H. Wang, and G. Oster. 1998. Energy transduction in ATP synthase. *Nature.* 391:510–514.

Engelbrecht, S., and W. Junge. 1997. ATP synthase: a tentative structural model. *FEBS Lett.* 414:485–491.

Farinas, J., and A. S. Verkman. 1999. Receptor-mediated targeting of fluorescent probes in living cells. *J. Biol. Chem.* 274:7603–7606.

Fillingame, R. 1990. Molecular mechanics of ATP synthesis by F_1F_o-type proton-transporting ATP synthases. *In* The Bacteria: A Treatise On Structure And Function. T. Krulwich, editor. Academic Press, London. 345–392.

Fillingame, R. H. 1996. Membrane sectors of F- and V-type H^+-transporting ATPases. *Curr. Opin. Struct. Biol.* 6:491–498.

Fillingame, R., W. Jiang, O. Dmitriev, and P. Jones. 2000. Structural interpretations of F_0 rotary function in the *Escherichia coli* F_1F_0 ATP synthase. *Biochim. Biophys. Acta.* In Press.

Finbow, M., and M. Harrison. 1997. The vacuolar H^+-ATPase: a universal proton pump of eukaryotes. *Biochem. J.* 324:697–712.

Forgac, M. 2000. Structure, mechanism and regulation of the clathrin-coated vesicle and yeast vacuolar H^+-ATPases. *J. Exp. Biol.* 203:71–80.

Futai, M., T. Oka, Y. Moriyama, and Y. Wada. 1998. Diverse roles of single membrane organelles: factors establishing the acid lumenal pH. *J. Biochem.* 124:259–267.

Gambale, F., H. A. Kolb, A. Cantu, and R. Hedrich. 1994. The voltage-dependent H^+-ATPase of the sugar beet vacuole is reversible. *Eur. Biophys. J.* 399–403.

Graham, L. A., and T. H. Stevens. 1999. Assembly of the yeast vacuolar proton-translocating ATPase. *J. Bioenerg. Biomembr.* 31:39–47.

Groth, G., and J. Walker. 1997. Model of the c-subunit oligomer in the membrane domain of F-ATPases. *FEBS Lett.* 410:117–123.

Harrison, M. A., M. E. Finbow, and J. B. Findlay. 1997. Postulate for the molecular mechanism of the vacuolar H(+)-ATPase (hypothesis). *Mol. Membr. Biol.* 14:1–3.

Holzenburg, A., P. C. Jones, T. Franklin, T. Pali, T. Heimburg, D. Marsh, J. B. C. Findlay, and M. E. Finbow. 1993. Evidence for a common structure for a class of membrane channels. *Eur. J. Biochem.* 213:21–30.

Israelachvili, J. 1992. *Intermolecular and Surface Forces.* Academic Press, New York.

Jencks, W. 1989. How does a calcium pump pump calcium? *J. Biol. Chem.* 264:18855–18858.

Junge, W., H. Lill, and S. Engelbrecht. 1997. ATP synthase: an electrochemical transducer with rotatory mechanics. *TIBS.* 22:420–423.

Kaim, G., and P. Dimroth. 1999. ATP synthesis by F-type ATP synthase is obligatorily dependent on the transmembrane voltage. *EMBO J.* 18: 4118–4127.

Kibak, H., L. Taiz, T. Starke, P. Bernasconi, and J. P. Gogarten. 1992. Evolution of structure and function of V-ATPases. *J. Bioenerg. Biomembr.* 24:415–424.

Kinosita, K., R. Yasuda, and H. Noji. 1999. F_1-ATPase: a highly efficient rotary ATP machine. *In* Essays in Biochemistry, Vol. 35. Portland Press, Ltd., London.

Lauger, P. 1991. *Electrogenic Ion Pumps.* Sinauer, Sunderland, MA.

Leng, X., M. Manolson, Q. Liu, and M. Forgac. 1996. Site-directed mutagenesis of the 100-kDa subunit (vphlp) of the yeast vacuolar (H^+)-ATPase. *J. Biol. Chem.* 271:22487–22493.

Leng, X. H., T. Nishi, and M. Forgac. 1999. Transmembrane topography of the 100-kDa a subunit (Vphlp) of the yeast vacuolar proton-translocating ATPase. *J. Biol. Chem.* 274:14655–14661.

Long, J. C., S. Wang, and S. B. Vik. 1998. Membrane topology of subunit a of the F1F0 ATP synthase as determined by labeling of unique cysteine residues. *J. Biol. Chem.* 273:16235–16240.

Margolles-Clark, E., K. Tenney, E. J. Bowman, and B. J. Bowman. 1999. The structure of the vacuolar ATPase in *Neurospora crassa. J. Bioenerg. Biomembr.* 31:29–37.

Muller, M., U. Irkens-Kiesecker, B. Rubinstein, and L. Taiz. 1996. On the mechanism of hyperacidification in lemon. *J. Biol. Chem.* 271: 1916–1924.

Nakamoto, R., C. Ketchum, and M. Al-Shawi. 1999. Rotational coupling in the F_0F_1 ATP synthase. *Annu. Rev. Biophys. Biomol. Struct.* 28: 205–234.

Nelson, N. 1992. Structural conservation and functional diversity of v-ATPases. *J. Bioenerg. Biomembr.* 24:407–414.

Noji, H., R. Yasuda, M. Yoshida, and K. Kinosita. 1997. Direct observation of the rotation of F_1-ATPase. *Nature.* 386:299–302.

Oster, G., and H. Wang. 2000. Reverse engineering a protein: the mechanochemistry of ATP synthase. *Biochim. Biophys. Acta.* In Press.

Peskin, C. S., G. M. Odell, and G. Oster. 1993. Cellular motions and thermal fluctuations: the Brownian ratchet. *Biophys. J.* 65:316–324.

Rastogi, V., and M. Girvin. 1999. Structural changes linked to proton translocation by subunit c of the ATP synthase. *Nature.* 402:263–268.

Risken, H. 1989. *The Fokker-Planck Equation.* Springer-Verlag, New York.

Sambongi, Y., Y. Iko, M. Tanabe, H. Omote, A. Iwamoto-Kihara, I. Ueda, T. Yanagida, Y. Wada, and M. Futai. 1999. Mechanical rotation of the c subunit oligomer in ATP synthase (F_0F_1): direct observation. *Science.* 286:1722–1724.

Scarborough, G. 1999. Structure and function of the P-type ATPases. *Curr. Opin. Cell Biol.* 11:517–522.

Schmidt, A. L., and D. P. Briskin. 1993. Energy transduction in tonoplast vesicles from red beet beta-vulgaris L. Storage tissue proton-substrate stoichiometries for the proton ATPase and proton PPase. *Arch. Biochem. Biophys.* 301:165–173.

Stevens, T., and M. Forgac. 1997. Structure, function and regulation of the vacuolar (H^+)-ATPase. *Annu. Rev. Cell Dev. Biol.* 13:779–808.

Stock, D., A. Leslie, and J. Walker. 1999. Molecular architecture of the rotary motor in ATP synthase. *Science.* 286:1700–1705.

Superkova, L., F. Supek, and N. Nelson. 1995. The *Saccharomyces cerevisiae* VMA10 is an intron-containing gene encoding a novel 13-kDa subunit of vacuolar H^+-ATPase. *J. Biol. Chem.* 270:13726–13732.

Taiz, L., and N. Nelson. 1996. Evolution of V- and F-ATPases. *In* Origin and Evolution of Biological Energy Conversion. H. Baltscheffsky, editor. VCH Publishers, Inc., New York. 291–305.

Valiyaveetil, F., and R. Fillingame. 1997. On the role of Arg210 and Glu219 of subunit a in proton translocation by the *Escherichia coli* F_OF_1 ATP synthase. *J. Biol. Chem.* 272:32635–32641.

Vik, S. B., and B. J. Antonio. 1994. A mechanism of proton translocation by F1F0 ATP synthases suggested by double mutants of the a subunit. *J. Biol. Chem.* 269:30364–30369.

Wang, H., and G. Oster. 1998. Energy transduction in the F1 motor of ATP synthase. *Nature.* 396:279–282.

Wu, M., J. Llopis, S. Adams, J. McCaffery, T. Machen, H.-P. Moore, and R. Tsien. 1999. Using targeted avidin and membrane permeant fluorescent biotin to study secretory pathway organelle pH regulation. *Chem. Biol.* 7:197–209.

Yasuda, R., H. Noji, K. Kinosita, F. Motojima, and M. Yoshida. 1997. Rotation of the γ subunit in F_1-ATPase: evidence that ATP synthase is a rotary motor enzyme. *J. Bioenerg. Biomembr.* 29:207–209.

Yasuda, R., H. Noji, K. Kinosita, and M. Yoshida. 1998. F_1-ATPase is a highly efficient molecular motor that rotates with discrete 120° steps. *Cell.* 93:1117–1124.

Yokoyama, K., Y. Akabane, N. Ishii, and M. Yoshida. 1994. Isolation of prokaryotic V0V1-ATPase from a thermophilic eubacterium *Thermus thermophilus. J. Biol. Chem.* 269:12248–12253.

Yokoyama, K., E. Muneyuki, T. Amano, S. Mizutani, M. Yoshida, M. Ishida, and S. Ohkuma. 1998. V-ATPase of *Thermus thermophilus* is inactivated during ATP hydrolysis but can synthesize ATP. *J. Biol. Chem.* 273:20504–20510.

Zimniak, L., P. Dittrich, J. P. Gogarten, H. Kibak, and L. Taiz. 1988. The cDNA sequence of the 69-kDa subunit of the carrot vacuolar H^+-ATPase. Homology to the beta-chain of F0F1-ATPases. *J. Biol. Chem.* 263:9102–9112.